High-resolution morpho-tectonic profiling across an orogen

Necea, D.

2010

document version
Publisher's PDF, also known as Version of record

3. Multiple dating approach: Infrared Stimulated Luminescence (IRSL), Apatite (U-Th)/He and Apatite Fission Track (AFT)

3.1. Introduction

In order to understand the overall evolution of an orogenic system through time, it is necessary to constrain the amplitude, timing and rate of processes taking place in the orogen itself, as well as in the adjacent sedimentary basins. The main target of this study is to reconstruct the syn- and post-orogenic evolution of the SE Carpathians by quantifying the vertical movements that generate the topography. The study area consists of a 175 km long W-E geological transect (A-A' profile in Fig. 3.1). This transect starts in the Transylvanian basin, passes the orogenic system, the eastward tilted strata of the Focşani basin and ends up in the flat dipping Holocene deposits in the basin centre.

Results from the geomorphological study (Chapter 2) provided information on the last phases of the orogenic evolution recorded during the Quaternary. Despite the good control obtained on the amplitude of the vertical motions, with maximum located at the orogen-foreland transition zone, less accurate is the time when they took place. In this regard, a new set of data is provided by applying infrared stimulated luminescence (IRSL) dating technique to loess sequences overlapping the different bedrock surfaces. These bedrock surfaces, e.g. monocline structure and river terraces, are geomorphological features created when the river incises into the rocks (Chapter 2). The altitude of each bedrock surface above the riverbed and its formation time are used to determine the river incision rate induced by the uplift and/or climate.

Geological data in the SE Carpathian orogen provide an incomplete chronology of different orogenic events, particularly the Middle Cretaceous (Aptian-Albian) shortening of the internal nappes, the Paleogene quiescence, the Miocene overthrusting of the external units and the Quaternary deformation of the orogen-foreland transition zone. (U-Th)/He and Fission-Track (FT) thermochronological dating methods have been applied to constrain better the timing and magnitude of these events. These two methods are unique dating tools used to reconstruct the cooling-burial history of rocks in the uppermost crust (<5 km). Apatite mineral has been used because it records the latest, youngest cooling histories as passes upwards through low closure temperatures of two systems, i.e. 75-45°C for (U-Th)/He and 110-60°C for apatite fission-track (AFT), respectively. These can be related to processes taking place during the orogenic cycle (Fig. 3.8). In an orogenic system, exhumation of rocks takes usually place as a result of interaction between tectonic, climatic and erosional processes.

◀ Figure 3.1
Location of samples analysed for luminescence (IRSL) and low-T thermochronology (AFT and U-Th/He methods). IRSL samples are represented by pink triangles, where FP stand for samples collected along the Putna river in the Focşani basin with Putna river and TO stands for those collected along the Olt river in the Transylvanian/Braşov basins. AFT and U-Th/He samples collected along the same profile as the IRSL ones are represented by red rhombus, where P stands for the Putna river and O for the Olt river.

3.2. Infrared stimulated luminescence (IRSL) method

3.2.1. Luminescence mechanism

Luminescence occurs in electrically non-conductive solids containing lattice defects and is illustrated by the energy-band model (Fig. 3.2; Wagner, 1998). A real imperfect crystal is characterized by an occupied valence band, an empty conducting band and an energetic zone in between (Fig. 3.2a) which contains atomic defects such as vacancies and chemical impurities (Wagner, 1998). These defects serve as traps for negative (electrons) and positive (electron holes) charges liberated from the lattice atoms by the natural occurring (ionizing) radiation. This radiation results from the natural radioactive decay of isotopes such as ^{238}U, ^{235}U, ^{232}Th, ^{40}K and ^{87}Rb, which are contained within the minerals. During the decay, these isotopes emit alpha (^{4}He) and beta particles, and photons (gamma rays; Aitken, 1998). This natural radiation (excitation phase, Fig. 3.2b) induces ionization in electrons, which are removed from their parent atoms, in the valence band, and are lifted into the conduction band. Here, they diffuse freely, most of them return to the ground state, while some of them are trapped by the negative charge deficits (electron traps). The holes remaining after removals of electrons are trapped as well by positive charge deficits (hole traps). The trapped electrons stay in the meta-stable state (Fig. 3.2c) until they are evicted by thermal or optical stimulation (Fig. 3.2d). The former is induced by heating the sample to ca. 450°C, while the latter by exposure to light of different intensity and wavelength. During the light stimulation phase, the trapped electrons are activated and recombine via the conduction band with the hole centres (luminescence

Figure 3.2

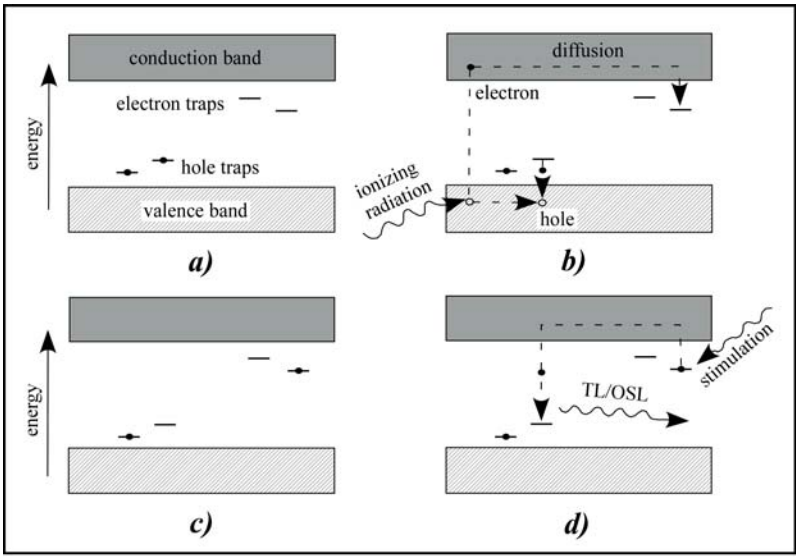

Energy band model of the luminescence phenomenon (after Wagner, 1998). (a) Ground state with empty charge traps, (b) ionizing radiation removes an electron from its parent atom and lifts it to the conduction band from where the electron is trapped, the remaining positive charge (electron-hole) is trapped at a hole trap, (c) metastable state with occupied charge traps, (d) the electron is liberated from its trap by thermal or optical stimulation and recombines with a hole centre (luminescence centre) under emission of luminescence (TL/OSL).

centres), emitting a beam of light, the so-called luminescence (Fig. 3.2d). The electron traps situated at deeper depths require a higher amount of activation energy in order to release the electrons. The shallow ones are released firstly and the deeper ones later.

In this study, infrared light with a wavelength of 880±80 nm was used to stimulate the feldspars, and therefore, the method is called infrared stimulated luminescence (IRSL).

Intensity of the luminescence signal is proportional to the number of trapped electrons within the mineral lattice and reflects the equivalent dose or paleodose (D_E). It increases with time, reflecting a longer exposure to the environmental radiation (annual dose rate). Aitken (1998) defined the equivalent dose (paleodose) as the laboratory dose of the nuclear radiation necessary to induce a luminescence signal equal with that acquired in situ by the mineral grains since their burial or after the most recent bleaching event. The natural dose-rate is the rate at which the energy is absorbed by a grain during its burial, which depends on the surrounding material to which it is exposed. It is proportional to the rate at which trapped electrons are accumulated in the crystal lattice. This dose-rate is defined as the energy absorbed per kilogram per time unit and its unit of measurement is Gray (Gy)/time unit, where 1 Gy = 1 J·kg^{-1}. The dose-rate can be expressed as well as Gray per thousand years (Gy·ka^{-1}) or as milligray per year (mGy·a^{-1}).

The age of the sediment can therefore be written as:

$$Age(t)[ka] = \frac{paleodose(equivalent\ dose)[Gy]}{(annual)\,dose\ rate[Gy/ka]} \qquad (3.2.1)$$

3.2.2. Resetting and anomalous fading

Resetting of the luminescence clock (bleaching) takes place when the luminescence signal is reduced to a value near to zero and occurs when the sample is exposed either to sunlight or to artificial light in the laboratory. The natural signal accumulated by the grains can be related to a particular event, which can be dated.

Anomalous fading is defined as the spontaneous decline of the luminescence intensity over time (in feldspar; Wintle 1973) and has been observed in freshly artificially irradiated samples. In order to verify the stability of the signal, fading tests are usually carried out by measuring the feldspar samples immediately after irradiation and later after being stored for several months. During this study, fading test measurements have been done for all samples only after irradiation, but unfortunately, they were not analysed and results can not be reported.

3.2.3. Determination of equivalent-dose or paleodose (D_E)

The equivalent dose can be estimated using three procedures: additive or total bleach, partial bleach (less applied) and regenerative (Forman et al., 2000). They define a DE from empirically derived functions based on the luminescence response of the sample to beta or gamma doses from calibrated radioactive sources and reduction of luminescence signal by laboratory light exposure. The additive and regenerative procedures (Fig. 3.4a-b) assume reduction of luminescence signal of mineral grains by sunlight or heat prior to deposition, to near a low definable level (Fig. 3.3). It increases exponentially over the geological time from near zero to a higher value due to the grain exposure to the natural ionizing radiation (Fig. 3.3; Huntley et al., 1985). This value is measured as the natural

luminescence signal at the moment when the sample is collected (Fig. 3.3).

3.2.3.1. Additive procedure

D_E is essentially calculated for this procedure (Fig. 3.4a) from two sets of data: (1) the residual luminescence level reached after a long laboratory light exposure assumed to be similar to the level attained prior to deposition and (2) a luminescence growth curve, which is the response of the sample to the additive beta or gamma radiation. Intensity of the luminescence signal is measured during the infrared stimulation (this study), resulting in a non-exponential decreasing shine-down curve (Fig. 3.5a). Its non-exponential character is due to the contribution of traps, which are difficult to be stimulated and to electron retrapping (Wagner, 1998). Huntley et al. (1985) show that the luminescence intensity plotted versus time increases as the age gets older (Fig. 3.5a). The luminescence

Figure 3.3

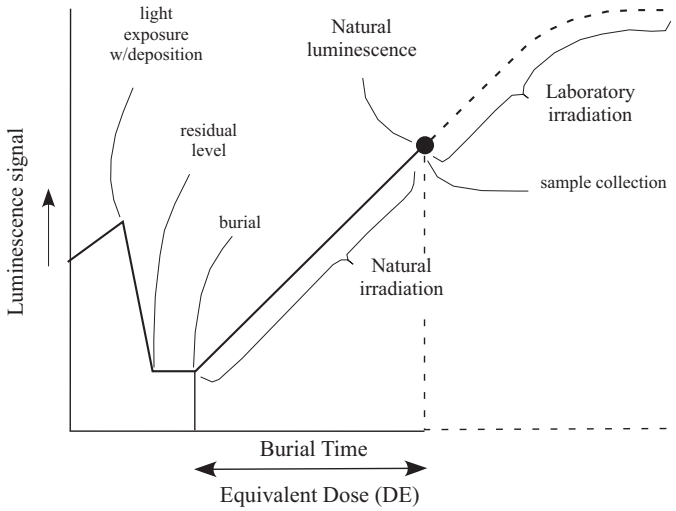

Luminescence geological cycle (after Forman et al., 2000). Light exposure reduces the luminescence signal of sediments to a low definable level. After the sediment burial, the ionizing radiation progressively imparts a luminescence signal. The signal at the collecting time is called the natural luminescence. Beta doses added to the natural signal defines a function, which is often the basis for determining the equivalent dose.

intensity shows a maximum value in the first few seconds since the measurement has started, decreasing progressively down to a value which remains invariable for the last 50-60 seconds (Fig. 3.5a). This is the residual signal that could not be removed during the laboratory bleaching and has to be subtracted (Aitken and Xie, 1992). Equivalent additive doses representing a certain number of measurements are plotted together in an additive growth curve (Fig. 3.5b). DE is then evaluated through the backward extrapolation of the luminescence intensity against the laboratory doses. It corresponds to the luminescence value at the intersection point with the equivalent dose (Fig. 3.4a; Forman et al., 2000). In general, the signals plotted versus doses should theoretically show a linear growth, but practically this aspect occurs only at the beginning or with very young samples. The curve will approach asymptotically to a saturation value (the line will be curved) when larger doses are involved or with older samples.

The equivalent-doses are plotted as well versus time after the laser was switched on,

Figure 3.4

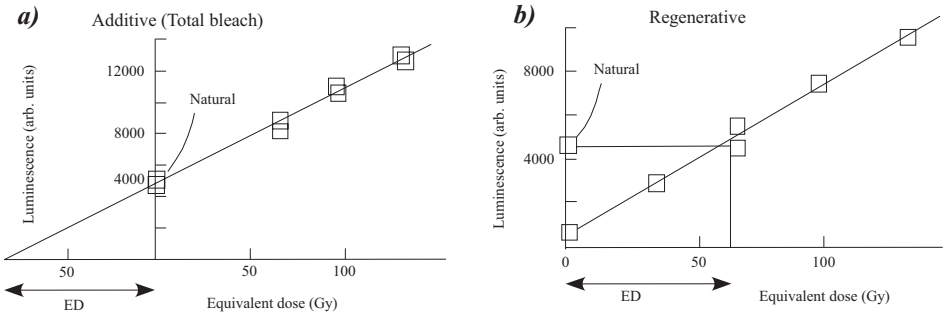

Graphic representation of (a) additive (total bleached) and (b) regenerative procedures, which are the most used to determine the equivalent doses for luminescence dating (discussion in text; after Forman et al., 2000).

resulting in an *equivalent dose plateau test* (Fig. 3.5c; Huntley et al., 1985). This shows if the sample was completely or partially bleached during its burial. If there is no constant equivalent dose with stimulation time, it indicates that the sample was insufficiently exposed to sunlight and less light-sensitive traps were progressively sampled.

3.2.3.2. Regenerative procedure

D_E is determined by comparing the natural luminescence signal to the luminescence signal that has been regenerated by the different additive laboratory doses, after extended light exposure (Fig. 3.4b; Forman et al., 2000). This procedure is applied to well light-bleached aeolian material in which the signal was reduced to a low residual level prior to deposition, a level which is redefined in the laboratory by exposure to ultraviolet light or to natural sunlight for more than 8 hours. If the sensitivity between the natural and the

Figure 3.5

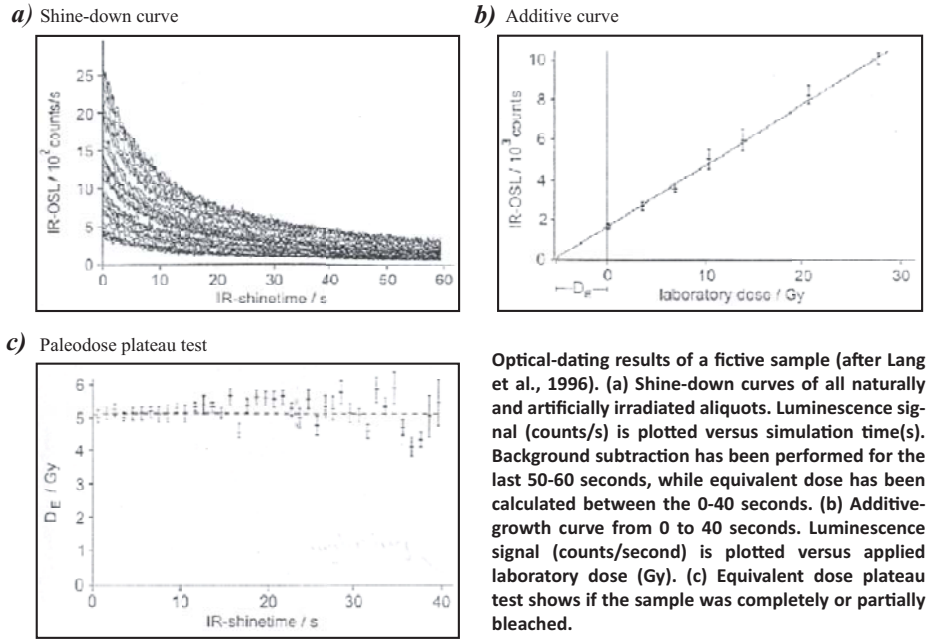

Optical-dating results of a fictive sample (after Lang et al., 1996). (a) Shine-down curves of all naturally and artificially irradiated aliquots. Luminescence signal (counts/s) is plotted versus simulation time(s). Background subtraction has been performed for the last 50-60 seconds, while equivalent dose has been calculated between the 0-40 seconds. (b) Additive-growth curve from 0 to 40 seconds. Luminescence signal (counts/second) is plotted versus applied laboratory dose (Gy). (c) Equivalent dose plateau test shows if the sample was completely or partially bleached.

regenerated signals is changing than the D_E will be erroneous and corrections have to be done. This procedure was not used during this study, further on being neglected.

3.2.3.3. Sample preparation procedure

The 22 samples collected from the SE Carpathians and adjacent basins (pink triangles along the A-A' profile in Fig. 3.1) are predominantly composed of loess and partially of fine sand, each weighing between 200 and 300 grams. Steel cylinders of 20 cm width were horizontally hammered into the sediment. Subsequent to recuperation, both ends of the cylinders were immediately covered with lightproof plastic lids to shelter the sample from exposure to the light. An additional sample of sediments from the same location was sealed in a plastic bag, which was used to determine the actual water content and to measure the present-day alpha-, beta- and gamma dose rates.

All samples were processed according to the standard sample separation procedure used at the Heidelberg luminescence laboratory (Lang et al., 1996). During the mineral separation, special attention was paid to the light and only Schilles red light was used (Schilles, 1998). This was never directly focused on the sample, allowing in this way for the minimum loss of the luminescence signal. In the lab's dark room, both ends of the cylinder were removed and about 1 cm of sediment was taken away from each end because the material could be exposed to the light losing the luminescence signal. The material remaining in the core of the steel cylinder was used further for the luminescence analysis.

In a first step, the material was separated by sieving in water, in three grain fractions: >212 µm, 125-212 µm and <125 µm. The first two fractions were dried in the oven at 50˚C and put aside. The fraction <125 µm was treated several times with 30% H2O2 in order to remove the organic material. Subsequently, it was treated with 20% acetic acid (Kadereit, 2000) for the lime to be removed and then roughly 40 ml of sodium oxalate was added to prevent sampling out in the next step with acetone. During this step, the grain size was significantly reduced, obtaining a fine-grained polymineral fraction of 4-11 µm. This fraction is used by the additive procedure (applied in this study) because the alpha particles penetrate fully the grains of this size, which is considered when the age is calculated. Formula from equation 3.2.2 is usually used to calculate the age, while formula of Kadereit (2000) was used in this study, which also considers the water content. 80 aliquots (aluminium discs) have been prepared by settling down in acetone suspension the 4-11 µm polimineral fraction, each aliquot carrying 1 to 2 mg of sediment. Infrared stimulation is applied to this fraction to probe the potassium-feldspar signal with blue emission (410 nm).

3.2.3.4. Measurements of D_E

The additive procedure has been used during this study, for which DE was obtained by following the Heidelberg laboratory protocol (Lang et al., 1996; Kadereit, 2000), which consisted in using the previously prepared 80 aliquots.

Prior to any analysis, test measurements were carried out for all 22 Carpathian naturally bleached samples in order to detect the natural luminescence signal by using 4 aliquots per sample. Two aliquots were irradiated, while the other two were used for measuring the natural signal. All 4 aliquots were short-shined for 0.4 seconds by infrared light at room temperature to normalize the aliquot signals. D_E obtained for each sample served to determinate the suitable amount of radiation later used to irradiate the sample. The test results show that depositional bleaching was acquired by the aeolian loess deposits, and therefore, the additive method was applied for age calculation. Deficiency of deposi-

tional bleaching was observed in the alluvial sandy deposits (half of the samples). This is represented by the DE values obtained for each sample, which are bigger than those that are published in the literature (e.g. deposits with comparable ages). It indicates that the sample exposure to the light was insufficient in order to eliminate the remnant natural IRLS signal and to reset the clock. These samples were disregarded from interpretation.

After the test measurements, the 11 good samples were further used for real measurements. The 76 aliquots left for each sample were firstly exposed to short-shine light. Ten aliquots from each sample were used to measure the natural luminescence signal, while the remaining 66 aliquots were separated in different groups. Nine aliquot groups (5 each; 45 in total) were artificially irradiated with a variety of laboratory beta doses, which were added to the natural signal. The applied beta doses had intensities up to six times the natural signal and calibrated Sr/Y-90-β-sources were used. Another 2 aliquot groups (5 each) were separated for fading tests, one group to be used for measuring the natural luminescence and another one to be irradiated. These aliquots suppose to show if the luminescence signal remained stable in time. The obtained measurements from the fading tests were not analysed during this study, and unfortunately, results cannot be reported. Additionally, 3 groups (3 aliquots each) were irradiated with alpha doses using an AM-241-α-source, the applied intensities being up to four times higher than the natural signal. The alpha irradiation was calculated assuming an alpha particle sensitivity of 7-10%. Subsequently, all the artificially irradiated aliquots were stored for more than six weeks in a dark place at room temperature to remove potentially unstable signals induced by the irradiation. Later, both beta- and alpha-irradiated aliquots were pre-heated at 220°C for 2 minutes to empty the shallow traps, and then, exposed for 60 seconds to infrared light (880±80 nm) at room temperature to empty the electrons from the traps. The 9-beta- and 3-alpha additive doses were measured for each sample, additive growth curves resulting from beta- and alpha-groups (Fig. 3.5b). The background subtraction was applied (Aitken and Xie, 1992) to each sample in order to remove the residual luminescence signal (for the last 50-60 seconds) and beta and alpha equivalent-doses were calculated between the 0-40 seconds (Fig. 3.5b; values in Table 3.1).

The measurements were performed using a Risø reader TL-DA-12 system (Bøtter-Jensen, 1988; Bøtter-Jensen and Mejdahl, 1984; Bøtter-Jensen et al., 1991; Markey et al., 1996) equipped with an EMI 9635Q photomultiplier in single photon counting mode and TEMT 484 diodes for intense (40 mW/cm²) infrared stimulation. G. Duller's ANALYSE software (1999) was used for data processing and R. Grün's SIMPLEX ROUTINE (1993) to calculate the equivalent-doses (exponential fit).

3.2.4. Determination of dose-rate (annual dose)

The annual dose or dose rate represents the total contribution of the alpha, beta and gamma dose-rates. The formula 3.2.1 can be written as:

$$Age(t) = \frac{D_E}{kD\alpha + D\beta + D\chi + Dc} \qquad (3.2.2)$$

where D_E is the equivalent dose, $D\alpha$, $D\beta$, $D\gamma$, Dc are the total alpha, beta, gamma and cosmic contributions, k is a time-dependent constant (Aitken, 1998). For a given amount of absorbed energy, the alpha particles will be less effective in inducing luminescence signal than lightly ionizing radiations. The measure of this poor effectiveness is expressed in the k-value (or a-value), which is in the range of 0.05-0.2. Those traps present in the

Table 3.1

Sample name	Sample depth (m)	Beta equiv. dose (DE) (Gy)	Alpha equiv. dose (DE) (Gy)	Water content (d) (%)	Cosmic rays (Dc) (mGy/yr)	Beta dose-rate (Dß) (Gy)	Alpha dose-rate (Da) (Gy)	Th (ppm)	U with Rd (ppm)	U without Rd (ppm)	Rd groupe (ppm)	K (ppm)	IRSL ages (kyr)	Errors (%)
TO2	2	158.1±11.2	2511.1±233.5	1.15	0.1985±0.01	1.728±0.09	11.126±0.58	10.339±0.40	2.519±0.82	2.324±0.42	2.460±0.11	1.815±0.11	46±5	11
TO3	5	313.7±19.1	5000±300	1.15	0.1618±0.01	1.583±0.08	8.076±0.42	5.739±0.24	2.060±0.66	1.969±0.26	1.508±0.07	1.396±0.08	123±11	9
FP1	5.5	200.2±6.2	2398.0±47.8	1.15	0.1467±0.01	1.842±0.09	11.891±0.61	11.357±0.44	3.335±1.08	3.163±0.57	3.235±0.14	1.951±0.12	50±5	9
FP2	3.5	114.6±31.8	1580.5±633.6	1.1	0.1677±0.01	1.943±0.10	12.704±0.66	10.354±0.41	3.270±1.05	3.315±0.57	3.194±0.12	1.925±0.12	28±9	30
FP3	2	72.1±4.4	1203.3±8.9	1.05	0.1858±0.01	1.982±0.10	11.884±0.61	11.039±0.41	3.588±1.15	3.274±0.53	3.426±0.13	1.982±0.12	17±2	10
FP6	5.7	98.2±8.0	1189.1±6.7	1.15	0.1491±0.01	1.739±0.09	10.185±0.53	0.063±0.34	2.367±0.80	2.255±0.39	2.179±0.10	1.928±0.11	29±3	11
FP7	4.5	43.1±2.8	561.6±170.8	1.1	0.1593±0.01	2.329±0.12	11.446±0.59	9.024±0.36	2.603±0.87	2.087±0.42	2.692±0.12	2.161±0.13	10±1	11
FP10	4	83.9±6.1	903.6±236.1	1.05	0.1686±0.01	2.259±0.11	14.864±0.76	9.913±0.38	3.864±1.22	3.617±0.58	4.192±0.15	2.376±0.14	16±2	13
FP11	3	54.2±5.6	974.3±59.0	1.05	0.1804±0.01	2.215±0.11	13.566±0.70	10.573±0.40	3.790±1.20	3.455±0.57	4.046±0.15	2.125±0.12	12±2	13
FP15	13	417.9±98.6	3091.1±1254.6	1.1	0.0989±0.01	1.316±0.07	8.051±0.42	5.728±0.17	1.606±0.58	1.769±0.27	1.691±0.05	1.166±0.04	148±42	29
FP16	1	101.5±14.1	1401.0±94.0	1.1	0.1998±0.01	1.708±0.09	11.101±0.57	9.949±0.39	2.622±0.87	2.848±0.51	2.475±0.11	1.735±0.11	28±5	16

Optical-dosimetric data and infrared stimulated luminescence (IRSL) ages. The beta- and alpha equivalent doses (DE) have been measured in the laboratory. The water content (δ in %) is the weight ratio between the wet and dry sediment. The dose-rate for cosmic rays (Dc) was calculated using the Kosmische-DL software of P. Karelin based on tables of Prescott and Hutton, 1994; Adamiec and Aitken (1998) and formulas of Aitken (1998). The dose-rates for beta, alpha and gamma rays (kDα, Dβ, Dγ) have resulted from measuring concentrations of Th-, U- and K- through ICPMS (Inductively Coupled Plasma Mass Spectrometer). All these data served to calculate the IRLS ages and relative errors bars.

central core of the alpha tracks will get saturated and a large amount of deposited energy will be lost. For determination of the alpha-dose rates of the surrounding medium, a Littlemore ELSEC 7286 counter with four counting positions was used. Beta counting was performed with a Risø GMM-25-5 beta counter with 5 counting positions. Determination of gamma-dose and elementary concentrations of ^{238}U (ppm), ^{232}Th (ppm) and ^{40}K (weight, %) were done using low level gamma-spectrometry (values in Table 3.1). Contribution of cosmic rays was calculated using the Kosmische-DL software of P. Karelin (for half depth), which uses the tables of Prescott and Hutton (1994); Adamiec and Aitken (1998) and formulas of Aitken (1998). The cosmic dose-rate of each sample has a value of 0.18 Gy/ka^{-1} for a depth of 1 m, which attenuates with depth, e.g. with 14% per meter in rock or sediment with density of 2 g/cm^{-3} (values in Table 3.1.).

Equation 3.2.2 above mentioned as an example for age calculation was improved by Kadereit (2000), additionally, the water content being considered. It refers to that content retained within the sediment and has to be determined before any age calculation because the water absorbs the radiation from the mineral sediment, inducing underestimations in the D_E values (Lian et al., 1995). During this study, the water content was measured prior to any analysis and represents the weight ratio between the wet and dry sediment (δ in %; Table 3.1). The obtained values were assumed to remain constant over the burial history. The computed ages range from late Middle Pleistocene (148±42 kyr) to Holocene (10±1 kyr), with 1 sigma error bars in the order of 11%, seldom of 30% (Table 3.1; description and interpretation in Chapter 4).

3.3. (U-Th)/He method

3.3.1. Principle of method and He-ingrowth

This method involves the measure of the ratio between the U and Th (parent nuclides) and the amount of alpha particles or Helium atoms (decay product) retained in minerals. Radioactive decays of ^{238}U to ^{206}Pb, ^{235}U to ^{207}Pb and ^{232}Th to ^{208}Pb result in production of eight, seven and six atoms of He, respectively. Although, decay of ^{147}Sm produces a small quantity of He, ^{147}Sm was neglected in the age calculation since the apatite mineral analysed in this study had in most cases extremely low concentration (e.g. below ICPMS detection level <1ppb). The total amount of ^{4}He nuclides (He-ingrowth) produced in a mineral within a given time *t* can be written as follows:

$$^{4}He = 8 \cdot {}^{238}U(e^{\lambda_{238}t} - 1) + 7 \cdot {}^{235}U(e^{\lambda_{235}t} - 1) + 6 \cdot {}^{232}Th(e^{\lambda_{232}t} - 1) \quad (3.3.1)$$

where ^{4}He, ^{238}U, ^{235}U and ^{232}Th refer to the present-day measured amounts (parent nuclides per gram of sample); *t* is the accumulation time (He age) in years; *λ's* are the decay constants for ^{238}U (λ_{238} = 1.55125 x 10^{-10}yr^{-1}), ^{235}U (λ_{235} = 9.84850 x 10^{-10}yr^{-1}) and ^{232}Th (λ_{232} = 4.94750 x 10^{-11}yr^{-1}). The coefficients that precede the U and Th abundances correspond to multiple alpha particles emitted by each of the decay series. If the standards units for ^{4}He are given in cm^{3}/g rock (STP) and those for parent nuclides in µm/g sample, equation 3.3.1 can be rewritten as (Geyh and Schleicher, 1990):

$$^4He = 22415 \cdot \begin{bmatrix} 0.0336 \cdot {}^{238}U(e^{\lambda_{238}t} - 1) \\ + 0.0298 \cdot {}^{235}U(e^{\lambda_{235}t} - 1) + 0.0258 \cdot {}^{232}Th(e^{\lambda_{232}t} - 1) \end{bmatrix} \quad (3.3.2)$$

The He production equation presumes secular equilibrium among all daughters in the decay chain, a condition applicable to the crystals formed before 350 kyr prior to the onset of He accumulation (Farley, 2002).

3.3.2. Alpha-ejection correction and analytical errors

Radioactive decay of uranium and thorium series emits alpha particles with high kinetic energies in the range of 4-6 MeV (Farley et al., 1996). The energy conferred to these particles at the time of formation make them travel at a certain distance (stopping distance - *S*) through the mineral lattice before they come to rest (Ziegler, 1977). This distance is a function of the initial kinetic energy of the alpha particle, chemical composition and density of the host mineral. Alpha-stopping distances for uranium and thorium series are between ~11 to ~34 µm. Within apatite, the mean stopping distances are for ^{238}U = 19.68 µm, ^{235}U = 22.83 µm, and ^{232}Th = 22.46 µm (Farley et al., 1996). A mean value of ~20 µm is commonly used.

At the time of formation, the retention of ^{4}He within the apatite grains will depend on the positions of the parent nuclides relative to the crystal edge (Fig. 3.6). Alpha particles are retained in the host mineral when the parent nuclides are located at distances greater than 20 µm from the crystal edge (Ehlers and Farley, 2003). Helium ejected out of the host mineral is implanted into the adjacent minerals and vice versa. In the case of apatites, with a relative much higher concentration of U-Th than average minerals, significant implantation takes only place in certain mineralogical assemblages rich in minerals such as biotite and zircon.

To correct for the lost of helium, the alpha-ejection correction is applied. Surface-to-volume crystal ratio determines the magnitude of the correction, known as the *Ft* factor. Monte Carlo modelling is used to calculate the total amount of the alpha-particles

Figure 3.6

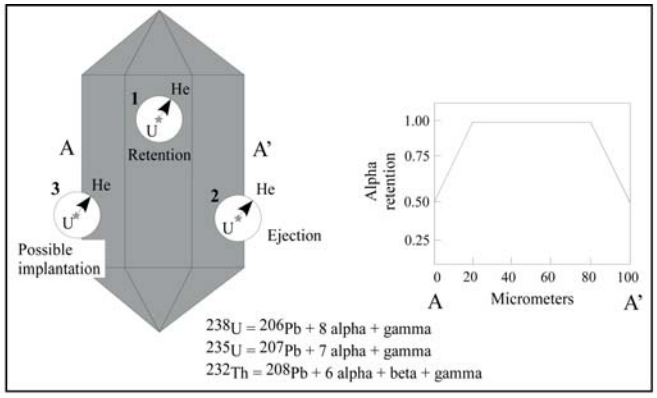

Three scenarios of alpha particles within an apatite crystal: (1) retention, (2) ejection and (3) possible implantation. A-A' is a cross-section through the crystal with maximum retention of alpha-particles between 20 and 80 µm (discussion in text; after Farley, 2002).

retained for a crystal with a homogeneous distribution of parent nuclides (Farley et al., 1996). In cases where a heterogeneous distribution is observed, numerical models can be applied (e.g. DECOMP, HeFTy) to stimulate the rate of diffusion. Farley and Stockli (2002) have shown that *Ft* for a grain with cross-section of 150 µm is close to 1 and decreases up to 0.7 for a grain of 50 µm. Grains with diameter of 75-150 µm retain 67% to 85% of the total He (Ehlers and Farley, 2003), while for 500 µm up to 97% is retained (Farley et al., 1996). In this study, the length and radius of analysed grains were between 100-200 µm and 40-80 µm, respectively (Table 3.2). The grains analysed in this study have had hexagonal geometries and only in some cases, spherical (Table 3.2).

For a spherical geometry of radius *R,* with stopping distance *S*, the *Ft* factor is computed as:

$$Ft = 1 - \frac{3S}{4R} + \frac{S^3}{16R^3} \tag{3.3.3}$$

For a grain with hexagonal geometry, the *Ft* is calculated by:

$$Ft = \alpha_1\beta + \alpha_2\beta^2 \text{ with } \beta = \frac{2.31L + 2R}{RL} \tag{3.3.4}$$

where, *α1* and *α2* are the fitting parameters incorporating the stopping distance and the density of the stopping medium (for ^{238}U: α1 = -5.13, α2 = 6.78, for ^{232}Th: α1 = -5.9, α2 = 8.99); *β* is the surface to volume ration (*S/V*) for a spherical or hexagonal geometry; *R* and *L* are radius and length of each analysed apatite grain. To calculate the mean *Ft*, a weighting factor (a_{238}) for the *Ft* values for U and Th is derived (Farley, 2002):

$${}^{mean}Ft = a_{238} \cdot {}^{238U}Ft + (1 - a_{238}) \cdot {}^{232Th}Ft \text{ with } a_{238} = \left(1.04 + 0.245\left(\frac{Th}{U}\right)\right)^{-1} \tag{3.3.5}$$

The He age divided by the correction factor yields the He-corrected age:

$$Corrected\ Age = \frac{Measured\ Age}{{}^{mean}Ft} \tag{3.3.6}$$

The length *L* and radius *R* of each grain was measured using micrometric scale during grain selection (Table 3.2). The *Ft* values obtained during this study vary from 0.569 to 0.811, with a mean value of 0.701 (Table 3.2). Error calculations have been done using an error propagation calculation of Juez-Larré and Meesters (oral communication, European Helium-Workshop, East Kilbride, 2004) based on the error analysis of Taylor (1997). This analysis allows estimating the propagation of the analytical (internal) and reproducibility (external) errors derived from the He, Th and U determination, and *Ft* correction.

3.3.3. He diffusion in apatite

Radiogenic daughter product (He nuclides) retained within the apatite grain can be easily lost by volume diffusion involving a single, thermally activated process. Thus, diffusivity is temperature dependent, and is characterized by an activation energy (E_a) and diffusivity at infinite temperature (D_o). This yields to an Arrhenius plot:

$$\frac{D}{a^2} = \frac{D_0}{a^2} \cdot e^{-Ea/RT} \tag{3.3.7}$$

where *D* is diffusivity, D_o is diffusivity at infinite temperature, E_a is activation energy, *R* is gas constant, *T* is temperature in Kelvin degrees and *a* is diffusion domain radius. If

Table 3.2

Sample name	Grain number	MWA length/radius (μm)	Radius Decomp	Grain geometry	^{4}He (atoms)	^{232}Th (atoms)	^{238}U (atoms)	Uncorr. age (Ma)	Ft	Corr. He age (±1s, Ma)
P4^	p1	109/54	54	hexagonal	4.52E+08	1.09E+12	4.83E+10	1.2±0	0.679	2±0
P4^	p3	134/59	61	hexagonal	4.52E+08	1.09E+12	4.83E+10	7.4±1	0.679	10±2[a]
P4^	p4	116/58	58	spherical	1.73E+08	1.41E+11	1.38E+11	0.8±0	0.721	1±0
P4*	p2	100/35	39	hexagonal	2.52E+08	8.26E+11	5.17E+10	0.8±0	0.569	1±0
P6*	p2	150/66	69	hexagonal	4.87E+09	6.30E+10	1.66E+11	20.8±2	0.764	27±4[o]
P7*	p1+p2+p3	110/46	49	hexagonal	7.48E+09	8.58E+11	2.98E+11	12±1	0.664	18±2
P7*	p4	137/53	57	hexagonal	3.94E+09	3.43E+11	2.68E+11	9±1	0.715	12±2
P8*	p1+p2	156/49	56	hexagonal	8.67E+09	3.73E+12	5.83E+11	5±0	0.691	7±1
P8*	p3	172/63	69	hexagonal	1.67E+10	8.36E+12	9.95E+11	4±0	0.744996	6±1
P9*	p1+p4	134/67	67	spherical	9.35E+09	1.24E+12	2.23E+11	14.2±1	0.743	19±2
P9*	p2	137/53	57	hexagonal	6.11E+09	1.13E+12	2.69E+11	9±1	0.705	13±2
P9*	p3	162/81	81	spherical	2.84E+09	7.65E+11	9.17E+10	8.2±1	0.783	11±1
P10^	p1	123/62	62	spherical	2.38E+09	9.75E+11	1.75E+11	4.6±0	0.723	6±1
P10^	p3	112/56	56	spherical	7.30E+08	1.30E+11	9.87E+09	14.2±1	0.692	20±2[a]
P10^	p4	131/66	66	spherical	1.22E+09	2.73E+11	1.20E+11	5.2±0	0.746	7±1
P10*	p2	96/48	48	hexagonal	3.29E+09	1.17E+11	6.01E+10	29.3±2	0.662	44±7[a]
P11*	p1+p3	150/52	58	hexagonal	4.31E+09	7.66E+11	2.49E+11	7.8±1	0.709	11±1[a]
P11*	p2	147/64	67	hexagonal	1.77E+09	1.10E+12	1.39E+11	3.5±0	0.739	5±0
P11*	p4	166/73	76	hexagonal	1.29E+09	6.74E+11	2.61E+11	2.4±0	0.777	3±0
P12*	p1+p3	165/44	52	hexagonal	5.75E+09	5.88E+10	2.26E+11	18.6±1	0.693	27±5
P12*	p2+p4	127/52	55	hexagonal	8.53E+09	8.08E+11	2.49E+11	15.2±1	0.698	22±3
P12*	p5	163/77	78	hexagonal	2.37E+09	3.67E+11	8.29E+10	11±1	0.779	14±2
P13*	p1+p3	117/42	46	hexagonal	1.49E+09	5.03E+11	1.03E+11	5±0	0.638	8±1
P13*	p2+p4	127/43	48	hexagonal	1.77E+09	1.92E+11	1.77E+11	6±0	0.668	9±1
P14*	p1+p3	129/50	54	hexagonal	2.17E+09	1.48E+11	1.54E+11	8.9±1	0.699	13±2
P14*	p2	163/63	68	hexagonal	1.31E+10	1.75E+12	8.99E+11	7.8±1	0.754	10±2
P14*	p4	114/50	52	hexagonal	1.46E+08	1.55E+11	1.22E+10	2.4±0	0.670	4±1
P18^	p1	163/52	59	hexagonal	1.01E+09	6.25E+11	2.05E+11	2.3±0	0.713	3±0
P18^	p2	189/57	66	hexagonal	7.72E+08	1.34E+11	6.44E+10	6.3±0	0.744	8±1
P18^	p3	177/54	62	hexagonal	1.77E+08	1.41E+10	1.37E+10	8.1±1	0.734	11±1
P18*	p4	128/49	53	hexagonal	5.35E+09	4.45E+11	3.65E+11	9±1	0.695	13±1
P18*	p5+p6	126/54	57	hexagonal	4.86E+09	1.23E+11	2.74E+11	12±1	0.717	17±3
P25*	p1+p4	113/44	48	hexagonal	2.23E+09	1.20E+11	1.81E+11	8±1	0.666	12±1
P25*	p2	128/44	49	hexagonal	4.36E+09	3.85E+11	3.78E+11	7±1	0.673	11±1
P25*	p3	137/60	63	hexagonal	3.27E+09	3.61E+11	1.90E+11	9±1	0.734	13±1
P26*	p2	126/49	53	hexagonal	2.14E+09	1.54E+10	6.06E+10	25.7±2	0.698	37±3
P26*	p4	115/48	51	hexagonal	6.18E+09	2.58E+11	1.44E+11	23.5±2	0.680	35±5
P27*	p1	217/80	88	hexagonal	8.80E+09	3.08E+11	7.51E+11	8.3±1	0.811	10±2
P27*	p2	156/74	75	hexagonal	3.21E+09	9.42E+10	4.02E+11	5.9±0	0.784	7±1
P27*	p3+p4	138/45	51	hexagonal	2.16E+09	6.92E+11	2.66E+11	3.9±0	0.675	6±1
P28^	p1	193/43	53	hexagonal	5.37E+09	6.16E+11	5.40E+11	6.1±0	0.689	9±1
P28^	p2	144/53	58	hexagonal	8.70E+08	3.32E+11	5.84E+10	5±0	0.704	7±1
P28^	p3	134/44	50	hexagonal	4.49E+09	4.15E+11	6.47E+11	4.7±0	0.678	7±1
P28*	p6	109/40	44	hexagonal	9.52E+08	8.03E+10	1.82E+10	20±2	0.622	32±3[a]
O1*	p1	197/64	72	hexagonal	5.07E+09	1.07E+10	2.86E+10	125.9±9	0.774	162±13[a]
O1*	p3+p4	112/43	47	hexagonal	6.83E+09	2.46E+11	2.41E+11	17.8±1	0.657	27±3
O1*	p5+p6	110/48	50	hexagonal	9.23E+08	1.63E+11	2.08E+10	12.3±1	0.660	19±2
O3*	p1+p2	144/50	56	hexagonal	5.23E+09	4.39E+10	2.32E+11	16.7±1	0.711	23±2
O3*	p3+p4	89/37	39	hexagonal	8.91E+08	2.03E+10	3.61E+10	16.9±1	0.606	28±2
O6*	p1+p2	116/36	41	hexagonal	8.23E+08	6.33E+10	3.05E+10	14±1	0.607	23±2
O6*	p3+p4	103/42	45	hexagonal	1.01E+09	8.45E+10	2.03E+10	20±2	0.631	31±3
O7*	p1+p2	123/52	55	hexagonal	1.45E+09	1.79E+11	7.79E+10	9.4±1	0.697	14±2
O7*	p3	188/45	54	hexagonal	2.52E+09	4.84E+10	3.26E+10	44.5±3	0.694	64±5
O7*	p4	163/77	78	hexagonal	1.28E+10	3.16E+11	1.28E+11	49.1±4	0.783	63±6
O8*	p1+p2+p3	107/38	42	hexagonal	2.78E+09	1.39E+11	2.84E+10	36±3	0.611	58±7
O8*	p4	168/44	52	hexagonal	7.32E+09	2.21E+11	1.26E+11	32±2	0.685	47±4
O8*	p5+p6	135/47	52	hexagonal	1.38E+09	1.52E+11	2.20E+10	19±2	0.672	28±4
O13^	p1	192/64	72	hexagonal	8.94E+08	1.41E+11	3.29E+10	10.6±1	0.760	14±1
O13^	p2	198/57	66	hexagonal	3.02E+09	4.08E+10	8.63E+10	24.4±2	0.752	32±4
O13^	p3	120/50	53	hexagonal	3.42E+08	7.45E+10	1.15E+10	9.3±1	0.678	14±1
O13*	p5+p6	115/41	45	hexagonal	9.80E+08	1.40E+10	1.85E+10	34.8±3	0.648	54±6

Single analysis (U-Th)/He ages computed for each sample (locations in Fig. 3.1). P4^ and P4* are samples which have been doubly analyzed for He content in laboratories from Glasgow and Amsterdam; p1-p5 are the analyzed apatite grains; MWA is the mass-weighted-average length/radius of crystal in aliquots; radius DECOMP is the grain radius used for modelling approximated to a spherical apatite with the same surface to volume ratio as the hexagonal grain; Ft is α-ejection correction using Meesters' Helium formula (Meesters and Dunai, 2002);

Figure 3.7

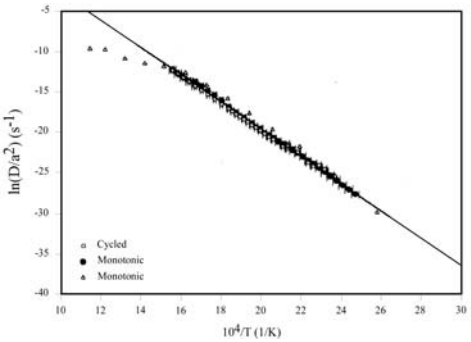

Arrhenius plot with helium diffusion data of a Durango apatite. The data show a linear array up to 300°C. Above this temperature, the apparent diffusion deviates from the straight line (discussion in text; modified after Farley, 2002).

Figure 3.8

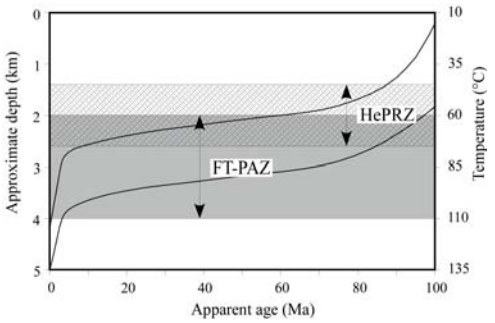

For an apatite mineral, the Helium Partial Retention Zone (HePRZ) and the Fission Track Partial Annealing Zone (FT-PAZ) are calculated based on a surface temperature of 10°C and a constant geothermal gradient of 25°C/km (modified after Farley, 2002).

this relationship is obeyed, then the measurements of $ln(D/a^2)$ will plot on a straight line with intercept $ln(D_0/a^2)$ and slope $-E_a/R$ (Fig. 3.7; Farley, 2002). Closure temperature can be computed from these two values.

Diffusion of helium out of the apatite grains is a result of the temperature and grain size (Fig. 3.8; Ehlers and Farley, 2003). The temperature at which helium is lost at a faster rate than it is produced is known as the closure temperature (Tc; Dodson, 1973). For the apatite (U-Th)/He system, this temperature is estimated around 75˚C. Helium is partially retained between 45-75˚C, namely the Helium Partial Retention Zone (HePRZ), and mostly retained below 45˚C. The use of these temperature benchmarks and the (U-Th)/He age allow to reconstruct the time-temperature path of a rock sample. With a good knowledge of the regional/local geology, rock cooling can be interpreted as a result of surface exhumation or changes in the geothermal field of the uppermost crust (1-4 km; Fig. 3.8).

The rate at which helium diffuses out of a grain can be influenced by factors such as He concentration gradient, grain size and morphology, degree of radiation damage (Zeitler et al., 1987; Lippolt et al., 1994; Wolf et al., 1996). The lost of helium leads to a reduction of the helium age (Meesters and Dunai, 2002) relative to the age of onset of cooling.

3.3.4. Inclusions

Fluid inclusions trapped during crystallisation of apatite minerals can introduce significant amounts of inherited helium, disrupting the initial concentration of He assumed to be zero. Solid inclusions tend to increase the heterogeneity in the distribution of the parent nuclides.

In this study, all grains were carefully scanned under the microscope and only inclusion-free grains were used for dating. Despite all, the poor reproducibility of some samples could be the results of the undetected micrometric inclusions. In those samples prepared for apatite fission-track analysis, it has been observed that many grains had zircon-inclusions, mineral with a high content in U and Th, which might induces an excess in He (parentless; Lippolt et al., 1994).

◀ Table 3.2 (continued)
uncorrected and α-corrected ages are in Ma with ±1 sigma error; [a] ages are much older due to the presence of the fluid inclusions, consequently, they have been neglected; [0] ages were neglected as well.

Figure 3.9

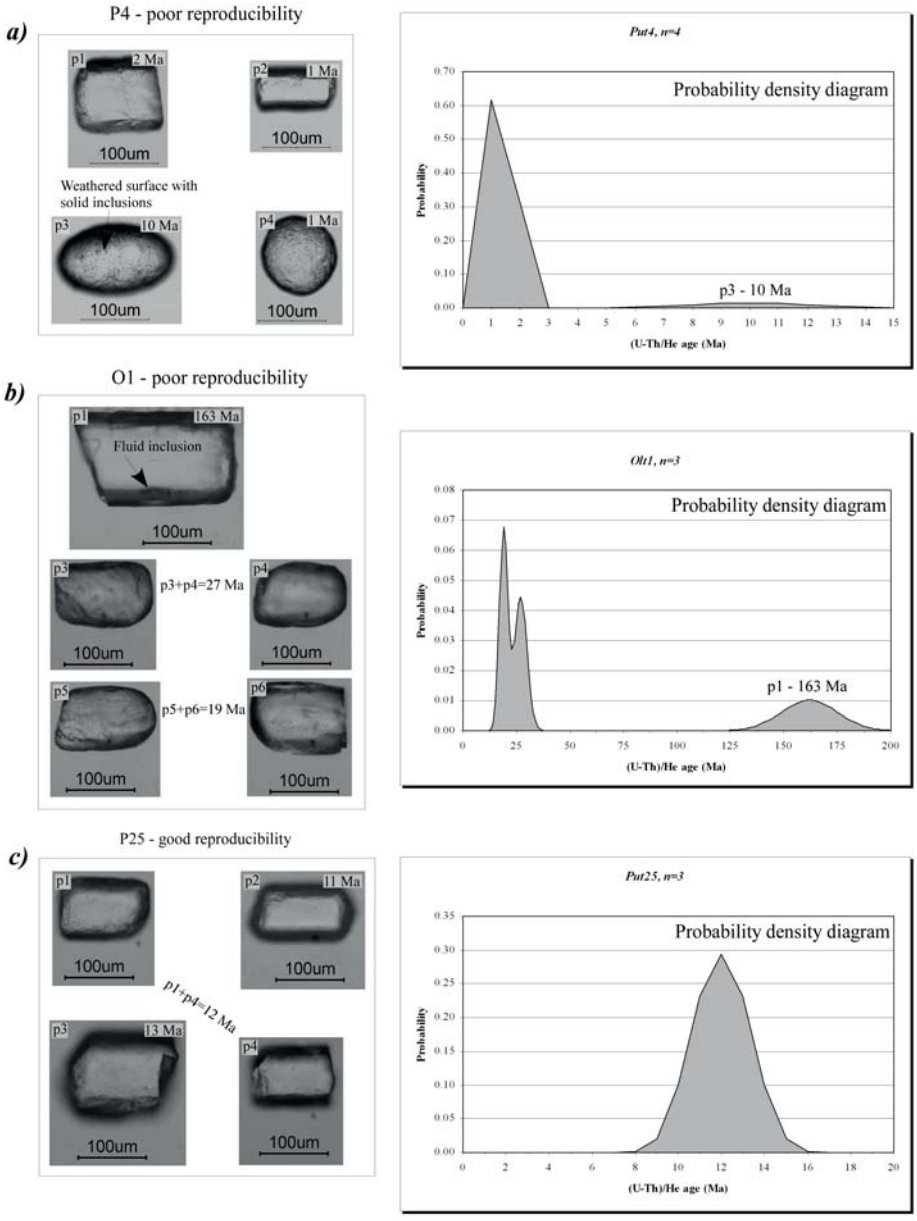

Presence of solid/fluid inclusions within the apatite grains leads to an excess of U, Th and He, which resulted in older erroneous He ages (a-b), while those grains without inclusions have similar single-grain ages (c). The erroneous He ages that occur as an isolated age in the probability density diagrams (PDD) computed for each sample have been neglected from He age calculation (details in Subchapter 3.3.9).

Table 3.3

Sample name	Weight (mg)	Added spike (gr)	^{4}He (cps)	^{4}He (atoms)	^{238}U (atoms)	^{232}Th (atoms)	Uncorr. He age (Ma)
Dur B2	0.028	0.06249	45709	1.78E+11	1.46E+13	7.03E+11	33.9
Dur B4	0.015	0.03570	22576	8.90E+10	7.57E+12	3.52E+11	32.9
Dur B7	0.034	0.02725	42546	1.68E+11	1.45E+13	6.52E+11	32.6
Dur B8	0.026	0.03524	36031	1.42E+11	1.21E+13	5.61E+11	32.8
Dur B9	0.015	0.03860	17487	6.79E+10	5.86E+12	2.69E+11	32.5
Dur B10	0.084	0.08592	176811	6.99E+11	5.55E+13	2.73E+12	34.9
Dur B12	0.006	0.02796	21058	8.19E+10	7.07E+12	3.18E+11	32.6
Dur B13	0.007	0.05048	20708	8.11E+10	6.93E+12	3.22E+11	32.8
Dur B14	0.049	0.04895	116115	4.61E+11	3.99E+13	1.80E+12	32.5
mean age of set 1							*33.1*
Dur1	0.010	0.03552	11381	4.45E+10	3.71E+12	1.52E+11	34.2
Dur4	0.014	0.04118	31132	1.25E+11	1.02E+13	4.58E+11	34.6
Dur5	0.030	0.08202	71377	2.85E+11	2.21E+13	1.10E+12	35.6
Dur6	0.017	0.05466	43085	1.71E+11	1.43E+13	6.72E+11	33.2
Dur7	0.087	0.08420	183937	7.47E+11	6.30E+13	2.75E+12	33.5
Dur9	0.045	0.05196	172560	6.95E+11	5.71E+13	2.54E+12	34.3
mean age of set 2							*34.2*
Durango mean age of both sets							**33.6**

Analytical data obtained for Durango standard. Two sets of analyses have been done prior and during the sample measurements, from which resulted a Durango mean age of 33.6 Ma (discussion in text).

3.3.5. He ages from Durango apatite used for calibration

In this study, aliquots of Durango fluorine-apatites were used (Young et al., 1969) to check the reproducibility of the analytical procedures used at the VU laboratory for (U-Th)/He dating. Analytical sensitivity to different amounts of U, Th and He was investigated by dating a large range of weights for various Durango aliquots. Results from Fig. 3.10a show that there is a good correlation between the amounts of He contents and the Durango weights (between 0.007-0.087 μgr). Results from fifteen aliquots yield ages between 32.5 and 35.6±3 Ma, nicely clustered around the regression line (Fig. 3.10b), with a mean age of 33±3 Ma (±2σ; Table 3.3). The calculated mean value is in good agreement with the He ages reported in the literature: 31.6±1 Ma (Jonckheere et al., 1993), 34±2 Ma (Wolf et al., 1996), 32.1±1.7 Ma (House et al., 2000); 32±1 Ma (Farley, 2002), 32.1±1.4 Ma (Persano et al., 2002). Previous studies carried out at the VU report Durango He ages of 33±2 Ma (Juez-Larré, 2003) and 32.1±2 Ma (Foeken, 2004). As the Durango samples have been measured prior to and in the same batch with the SE Carpathian samples (Fig. 3.1), the Durango ages give a good approximation on the reproducibility error before the α-corrections.

3.3.6. Sample preparation procedure

Three to four kilograms of rock sample were used to obtain enough apatite minerals for the (U-Th)/He and fission-track analyses. Rock samples were processed according to the standard sample separation and mineral treatment procedures used at the VU laboratory (Fig. 3.11). Samples were splitted and crushed using hydraulic presses, a jaw crusher and a disc mill. After each step, the obtained material was sieved at 250 μm, in order to avoid damaging the apatite grains already released from the host rock. The fraction <250 μm was soaked in a Na-pyrophosphate solution for at least 24 hours at room temperature and subsequently washed with water in order to remove the clay-seized fraction (e.g. <30 μm). The cleaned mineral fraction (30-250 μm) was dried in the oven at temperature below 40°C. Several heavy liquids and overflow centrifuging was used to

Figure 3.10

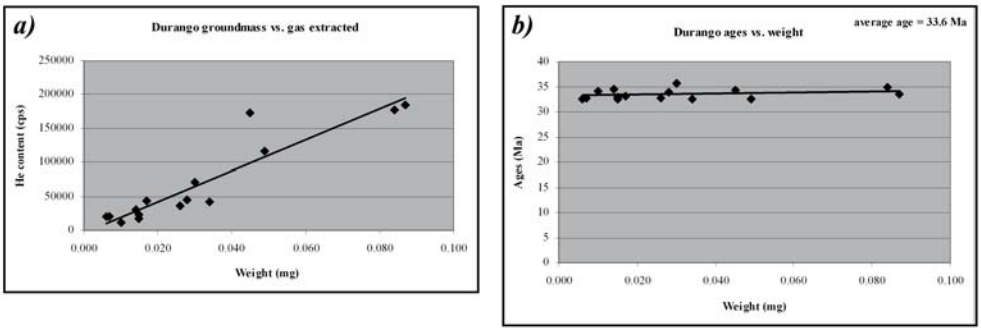

Analytical data of Durango standards obtained from 15 analyses measured during July-November 2006. (a) Relationship between the Durango groundmass (weight) and the gas extracted (He content), (b) Durango ages plotted vs. weight, from which resulted a mean age of 33.6 Ma (discussion in text).

Figure 3.11

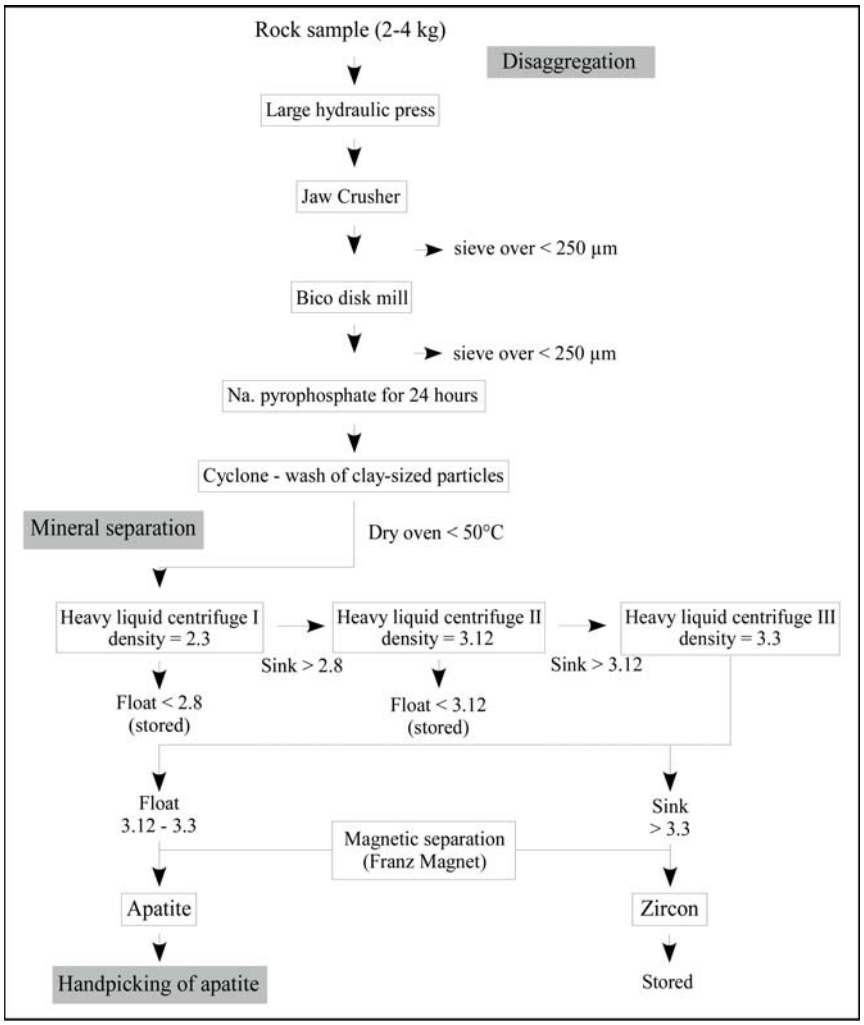

Flow chart shows different steps used during the mineral separation (after Juez-Larré, 2003; discussion in text).

separate the apatite from the lighter mineral fraction (IJlst, 1973), using the density characteristics of apatite (ρ = 3.19 g/cm^3; Fig. 3.11). Sample bulk with a density ρ < 3.00 g/cm^3 has been removed using di-iodmethane (CH_2I_2; ρ = 3.00 g/cm^3), while that with a density ρ > 3.00 g/cm^3 has been additionally treated twice with di-iodmethane, densities of ρ = 3.12 and ρ = 3.30 g/cm^3, respectively. It resulted a fraction with densities between 3.12 g/cm^3 and 3.30 g/cm^3, which has been finally proceeded with low to absent magnetic susceptibility of apatite. Frantz magnet was used to remove magnetic minerals from the heavy mineral fraction containing paramagnetic apatites. Finally, the best apatite minerals were selected by handpicking. The apatite mineral fraction was submerged in alcohol and inspected under a microscope using transmitted light (magnification up to x500). Apatite grains were handpicked based on their idiomorphic shape, lack of fractures and lack of fluid/solid inclusions. Four to six grains were selected per each sample. Each apatite was photographed and measured in order to apply the α-ejection correction (Farley et al., 1996; Farley, 2002; Farley and Stockli, 2002). More details about mineral separation techniques and equipment can be found at: http://www.falw.vu.nl/nl/opdrachtgevers/labs-aardwetenschappen/fysisch-laboratorium/mineral-separation-laboratory/index.asp.

3.3.7. Mass spectrometry

3.3.7.1. Helium extraction and analysis

For the He extraction, the handpicked apatites were loaded under the microscope in small Inconel cups, 9 mm in diameter and 8 mm high. Each cup was mounted in a holder equipped with a lid. The holder containing the capsule was inserted in a multiplexer equipped with five inconel arms held at Ultra High Vacuum (UHV) conditions (e.g. <10^{-9} mbars).

Most of the samples have been analysed at the noble gas laboratory of the VU Amsterdam (Table 3.2; www.falw.vu/~noblegaslab/lab/index.html), while another five at SUERC (East Kilbride, Glasgow, Scotland; www.gla.ac.uk/suerc/isogeosci/noblegas/helab.html). Each capsule was heated at 950°C for 35 minutes using a convection oven. The helium released was cleaned at UHV using a series of getters: Al-oxide getter at liquid nitrogen temperature, SAES 707 getter at 450°C and at room temperature, and zeolites. After the cleaning procedure, the helium gas was expanded into the mass spectrometre for analysis. Three mass points (3.9, 3.95 and 4.0) were measured in a 100 cycles loop. He abundance has been obtained by comparison with measurements of a internal helium standard (Table 3.2.). Second extraction of He was carried out for some samples to check for He excess derived from inclusions. The five samples measured at SUERC followed a similar analytical procedure as the one describe above, except that Helium was extracted by laser heating (Balestrieri et al 2005; Foeken et al., 2006).

3.3.7.2. U and Th analyses

Following the He extraction, the apatite grains were placed in Teflon (PFA) beakers and spiked with two artificial isotopes (^{230}Th and ^{233}U). The apatites were dissolved using 5 drops of concentrated HF 40% and 2 drops of concentrated HNO_3, the beakers were sealed and left overnight on a hot plate held at 120°C. Two and respectively one more drops of concentrated HNO_3 were added. Additionally, 0.6 ml 2.0N HNO_3 was added to assure the complete dissolution of the apatites and 1.4 ml of MilliQ-water to dilute them.

Figure 3.12

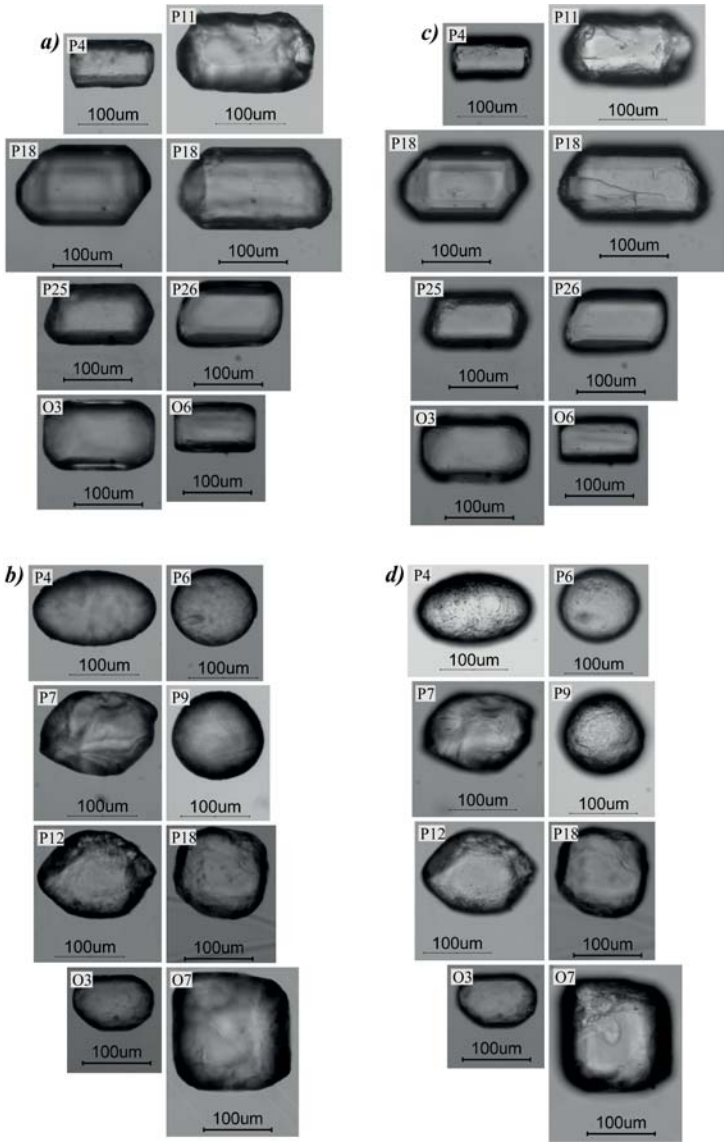

Morphologies and surface textures identified within the analysed apatite grains. (a) Grains with euhedral, sub-euhedral and rare angular geomorphologies (type one) occur dominantly in the Cretaceous flysch of the internal Carpathian units, the Paleogene rocks of the Tarcău nappe and the Upper Miocene-Pliocene sediments of the Focşani basin. (b) Rounded, sub-rounded and angular shapes (second type) are more abundant in the Marginal Folds and Subcarpatian nappes (external nappes). (c) Surface textures specific to the first morphologic type are: old reworked and new conchoidal fractures, steps and big grooves. (d) Textures corresponding to the second type are: upturned plates, etch-pits, small grooves, hollows resulting from natural degradation (description in text).

For those samples measured in Glasgow, 1.4 ml MilliQ-water and 0.6 ml 2.0N HNO_3 have been added, the beakers remaining for 2 days on the hot plate held at 80°C. A final 2 Normal HNO_3 solution was prepared for determination of U and Th, using a Thermofinnigan X series II Inductively Couple Plasma Mass Spectrometre (ICP-MS) at the Vrije Universiteit Amsterdam (Table 3.2).

3.3.8. Morphologies and surface textures of apatite grains

Morphologies and surface textures of apatite grains can reveal useful information regarding the number of apatite populations, source areas, grain transport and deposition (Krinsley and Doornkamp, 1973; Mahaney, 2002; Moral-Cardona et al., 2005). Krynine (1946) shows that apatites with euhedral forms have an igneous origin, while the rounded ones indicate erosion and transport as sediments.

Two morphological types have been recognized along the W-E profile (Olt-Putna profile), the first one consisting of euhedral, sub-euhedral and rarely angular forms (Fig. 3.12a), while the second one is determined by the rounded, sub-rounded and angular shapes (Fig. 3.12b). The former occurs dominantly in the Middle-Upper Cretaceous post-tectonic flysch covers from the Bucovinian, Baraolt and Ceahlău nappes (O6-O13) and the Paleogene sandstones from the Tarcău nappe (P25-P28; Fig. 3.12a). It has been less recognized further to the east in the conglomerates and sandstones from the Marginal Folds and Subcarpathian nappes (P4-P10), where the second morphological type is more abundant. Both types occur equally further eastward in the Upper Miocene-Pliocene clayey-sandy rocks of the Focşani basin (P11-P14; Fig. 3.12b).

Apatite surface textures observed in the two morphological types are different. In the first one, it dominates the old reworked and new conchoidal fractures, steps and big grooves (Fig. 3.12c), which indicates a short distance transport followed by deposition in the basin. In the second type occurs predominantly upturned plates, etch-pits, small grooves, hollows (Fig. 3.12d), which points to a longer distance transport between the source area and the deposition place.

Based on the abovementioned, it can be speculated that there are two apatite populations, each probably with a different source area. The euhedral apatites identified along the entire profile might originate in the volcanic rocks. Some of them probably belong to the Neogene-Quaternary volcanism (20-0.2 Ma) from the Harghita and Perşani mountains, which could be deposited only in the external nappes and the foreland basin during and post-Miocene shortening. The rounded apatites showing a longer distance transport might be placed possibly everywhere, but a westward source from the crystalline rocks and the Cretaceous flysch of the internal orogenic units might be suggested.

3.3.9. Probability density distribution (PDD) diagrams

The He-ages obtained for the SE Carpathian samples (red rhombus in Fig. 3.1) show a range of ages between 162±13 and 1±0 Ma (Table 3.2). PDD diagrams are used to display the age frequency and distribution. These diagrams produce a density estimation of the sample distribution using a Gaussian kernel (Sircombe, 2004). Its shape, the kernel, is narrow for ages with small errors, becoming wider for those with bigger errors. The peak shape depends on the age dispersion between grains as well as the error in age.

Single grain ages from each sample are present in the PDD diagrams in Fig. 3.13a-b. Single grain ages with comparable values from different samples overlap nicely within the ±2σ error yielding a PPD diagram with a single peak (P4, P8, P13, P25 and P26 in Fig. 3.13a; O3 in Fig. 3.13b). Some samples show PDD diagrams with two or three noticeable picks, but still connected under a bigger envelope (P7, P9, P12, P14 and P27 in Fig. 3.13a; O6 and O8 in Fig. 3.13b). Significant age dispersions can be observed in samples with two to four picks (P10, P11, P18 and P28 in Fig. 3.13a; O1, O7 and O13 in Fig. 3.13b),

Figure 3.13a

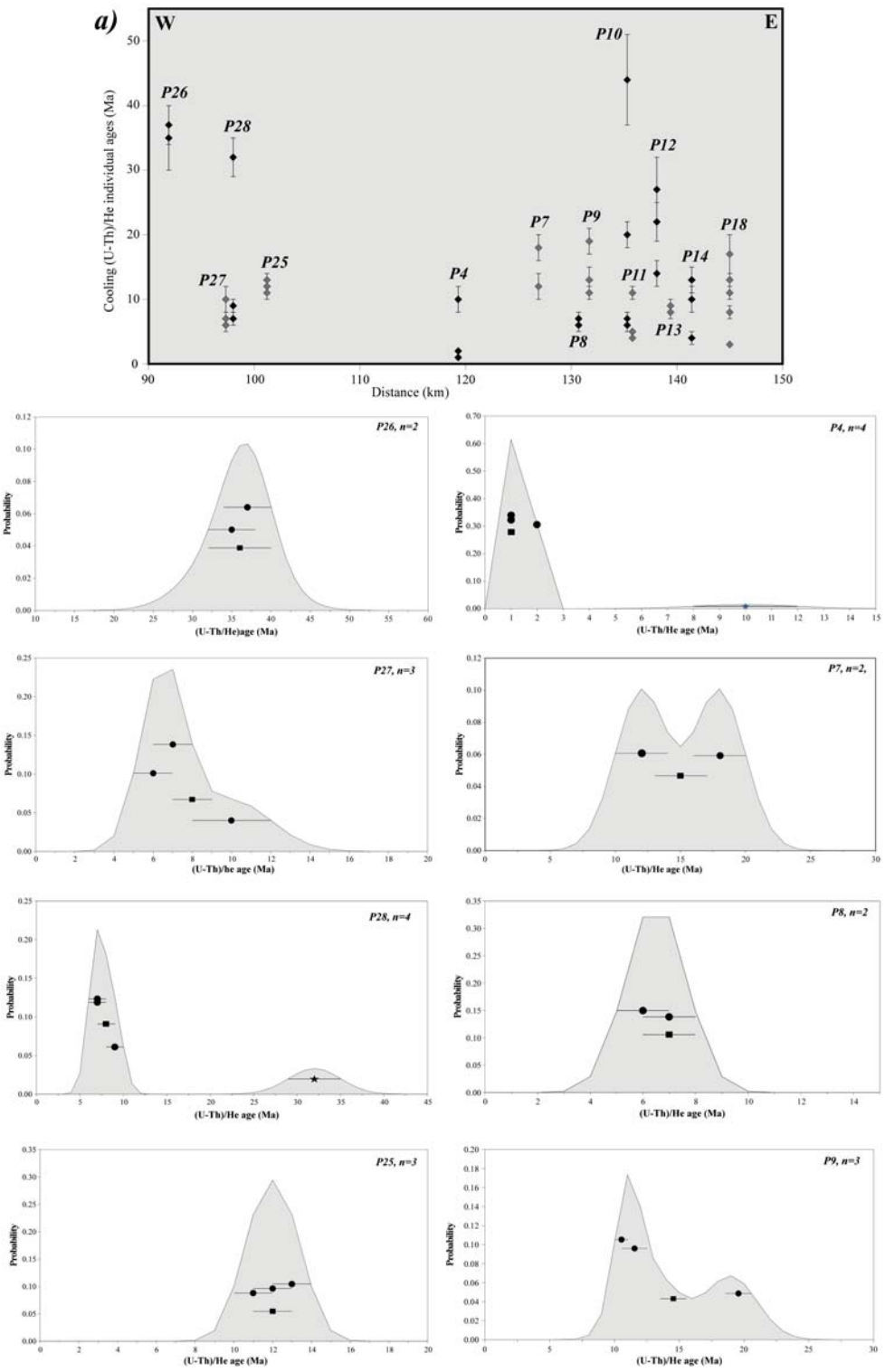
a)
W
E
Cooling (U-Th)/He individual ages (Ma)
Distance (km)
P26
P28
P27
P25
P4
P7
P9
P10
P12
P11
P8
P13
P14
P18
P26, n=2
P4, n=4
P27, n=3
P7, n=2,
P28, n=4
P8, n=2
P25, n=3
P9, n=3
Probability
(U-Th/He)age (Ma)
(U-Th/He age (Ma)
(U-Th)/he age (Ma)
(U-Th)/He age (Ma)

Figure 3.13a (continued)

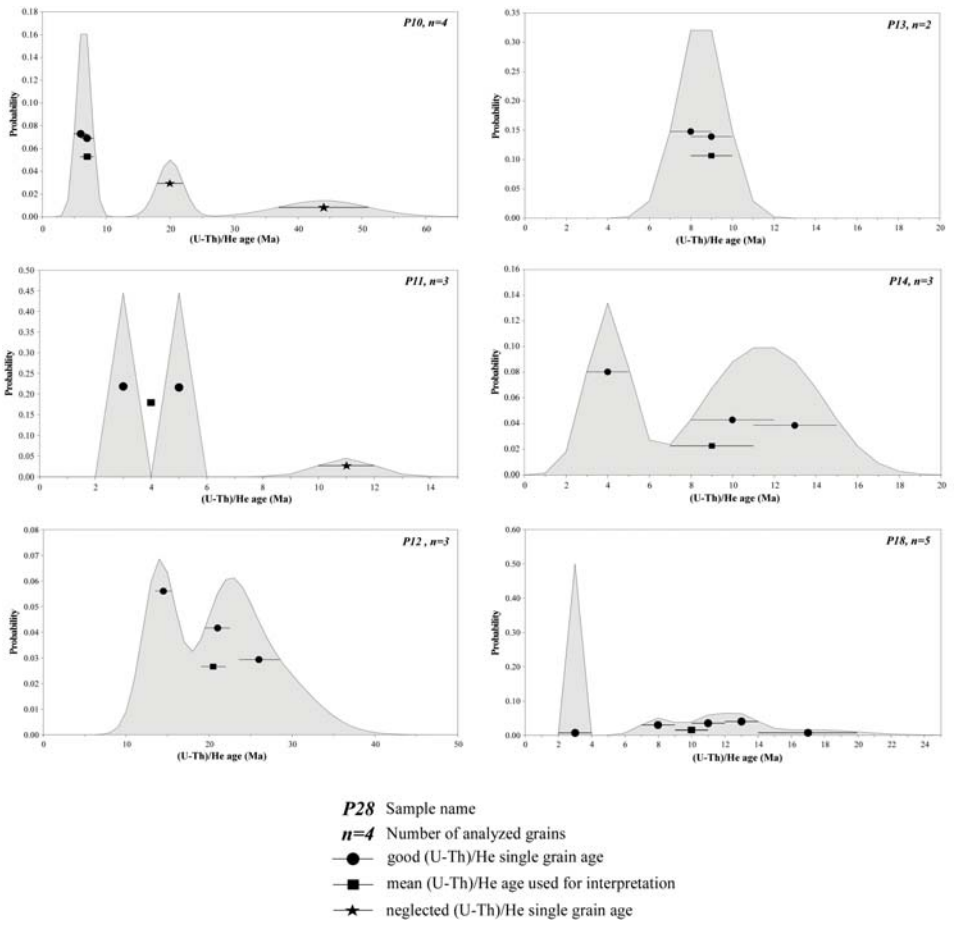

(U-Th)/He single analysis ages computed for samples collected along the (a) Putna and (b) Olt river profile segments. In the top chart, the samples are plotted vs. distance from west to east, while the underneath charts correspond to the probability density distribution diagrams (PDD) used to evaluate and display the ages obtained for each sample (description in text).

Table 3.4

Standard apatite Fish Canyon	Age ± 1sigma (Ma)	Irradiation date	Grain number	ρd (Nd) (CN5)	ρs (Ns)	ρi (Ni)	P(X2) (%)	Zeta ± 1sigma
FC3_I	27.9 ± 4.0	12/03/99	20	9.035 (8303)	1.712 (120)	9.787 (686)	97.8	353.9 ± 35.8
FC3_II	27.9 ± 3.0	12/03/99	30	9.035 (8303)	2.071 (225)	10.511 (1142)	99.2	314.2 ± 23.8
FC3_I	27.9 ± 2.9	21/05/99	31	8.825 (8201)	2.146 (240)	10.704 (1197)	99.8	316.0 ± 23.3
FC3_II	27.9 ± 3.2	21/05/99	32	8.825 (8201)	1.777 (194)	9.837 (1074)	70	346.9 ± 28.0
FC3_III	27.9 ± 3.4	21/05/99	27	8.825 (8201)	1.712 (166)	9.738 (944)	100	356.4 ± 30.9
					Weighted mean			**337.5 ± 28.4**

Personal zeta (ζ) calibration for dosimeter glass CN5 was performed on an apatite standard (Fish Canyon; five analyses). Nd, Ns and Ni are the number of glass dosimeter, spontaneous and induced tracks and σ is the standard error. ρd, ρs and ρi are the respective track densities, in 10^6 tracks/cm^2. P(χ2) is the Chi-squared probability of the single-grain ages in %. Weighted mean ζ resulted from the arithmetic average.

Figure 3.13b

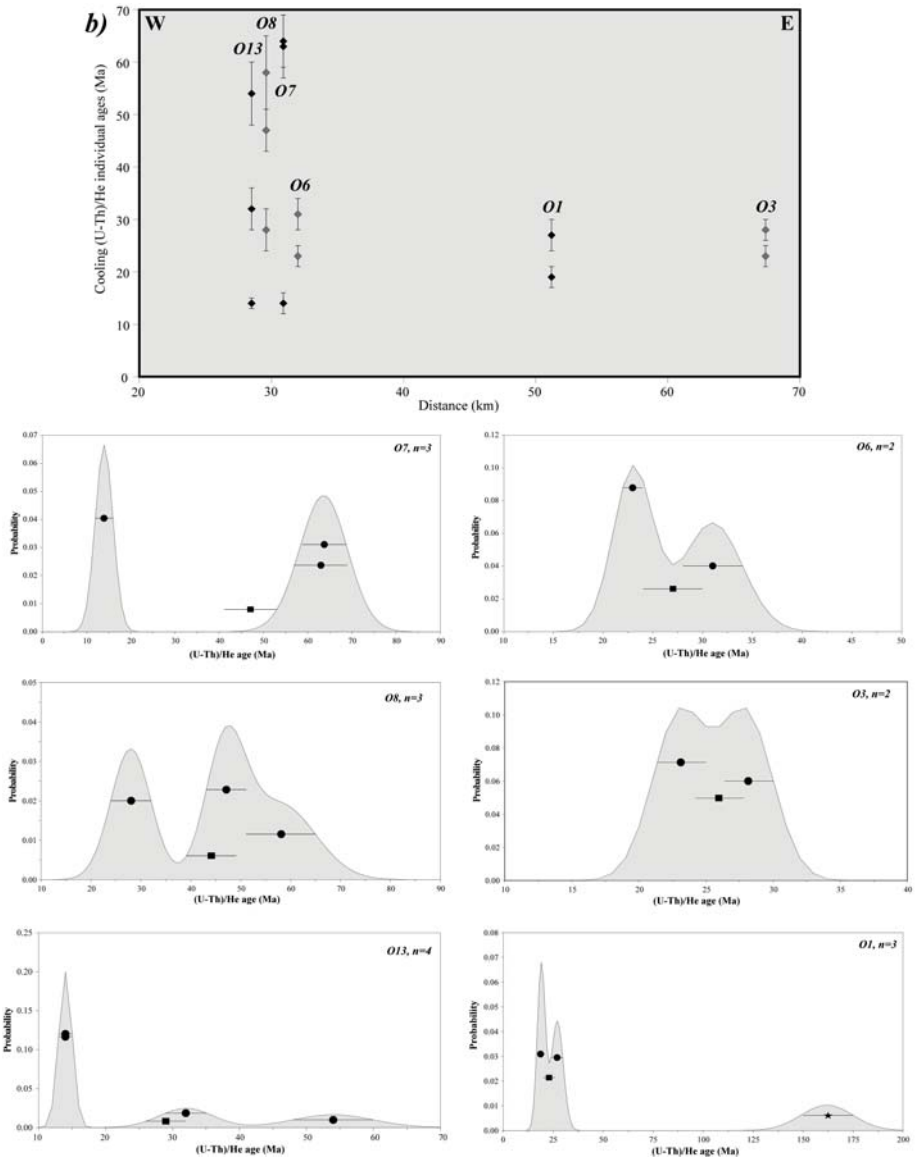

For description see Fig. 3.13a

which indicate that the He-ages do not belong to one population. This can be the result of different source areas and/or apatites with different diffusion rates. This latter is likely caused by the presence of the solid/fluid inclusions and/or heterogeneous distribution of parent nuclides.

3.4. Apatite Fission-Track (AFT) method

3.4.1. Fission-track formation

Radioactive elements present in the crystal lattice of minerals are unstable due to their atomic structure (Fig. 3.14a). Tracks form as a result of spontaneous decay of ^{238}U by fission. Because ^{238}U has the highest rate of decay by fission relative to the other elements, it can be considered as the main producer of tracks. During fission, the nucleus splits in two highly positive charged particles releasing energy of ~200 MeV. These two particles are ejected in opposite directions. In their passage through the host mineral, the nuclides interact with other atoms from the crystal lattice causing electron striping and ionization. Hence, the nucleus capture electrons and their energy is reduced until they come to rest, leaving a linear zone of damage, named fission-tracks (Fig. 3.14b-c). This model, known as the ion spike explosion model, is commonly used to explain formation of fission-tracks (Fleischer et al., 1975). In the case of ^{238}U in apatites, the fission-track is formed with an initial length of ~16 microns and a width of 25-50 angstroms (Å). Because of their small size, the fission-tracks can be enlarged by chemical etching, making possible to be observed under a microscope (Wagner, 1968; Wagner and van den Haute, 1992; Donelick et al., 1999).

Figure 3.14

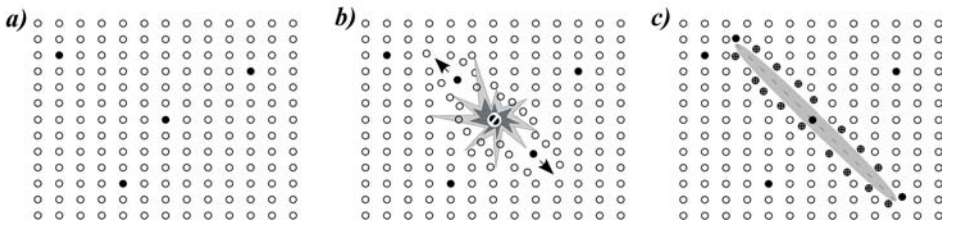

Cartoon representation of the ion spike explosion model for formation of fission-tracks in a mineral. (a) Trace amount of radioactive 238U is present in the crystal lattice (black circles), which is unstable due to its atomic structure. (b) Spontaneous fission of 238U results into two positively charged particles with equal mass, which recoil and travel in opposite direction. They interact with other atoms in the crystal lattice by electron striping and ionization, which leads to further deformation. (c) Gradually, the energy is reduced until the atoms come to rest, leaving a linear damage zone or fission-track (grey cylinder). It is visible optically after chemical etching (modified after Gallagher et al., 1998; Hendricks, 2003; Foeken, 2004).

3.4.2. Fission-track annealing and controlling factors

Fission-tracks are recognized to be metastable over their lifetime because they tend to be repaired naturally (shorten) until they disappeared as a result of the process known as “annealing” (shortening). Tracks are formed at a constant rate over time. A fission-track starts to anneal since the time of formation. As a result, it will experience a certain shortening and the resulting length is *l*. The degree of annealing is given by the l/l_o ratio. Ideally, the track lengths should be measured on surfaces parallel to the c-axis of the crystal and on tracks that are completely contained within the host mineral (confined track lengths) because they give the most accurate representation of the true track length distribution (Gleadow et al., 1986). The more individual track lengths are measured in a sample the better precision of length distribution will be gained. Annealing of fission-

Figure 3.15

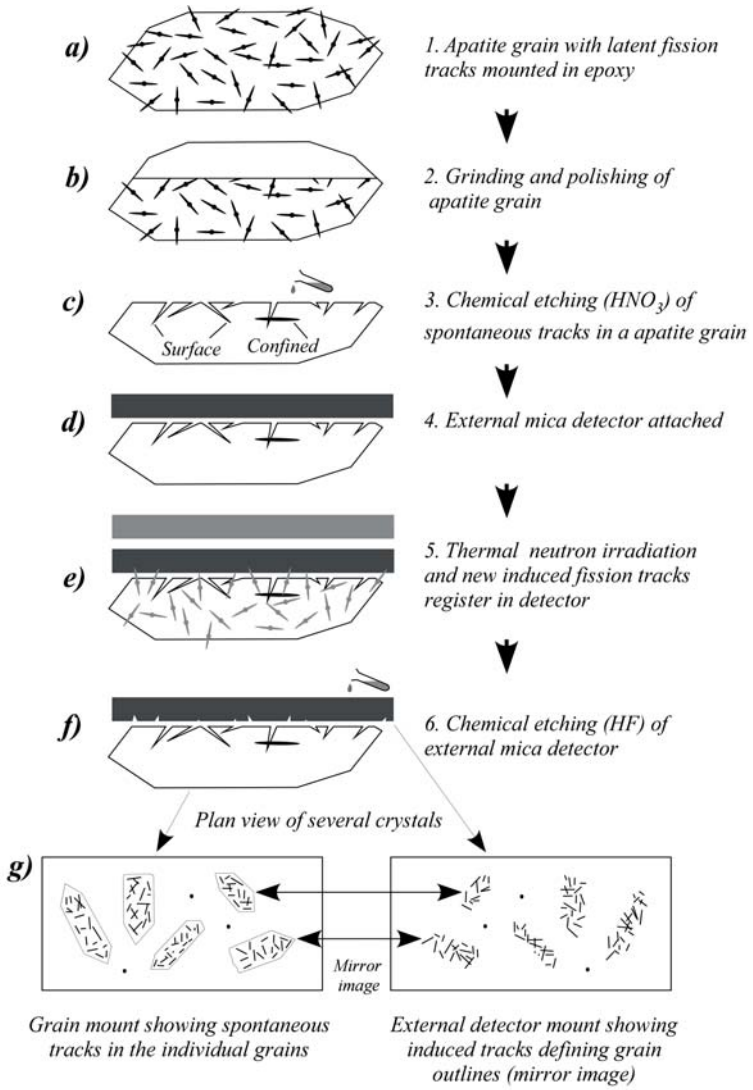

Laboratory steps involved in the External Detector Method. (a) Apatite grains with latent fission-tracks have been mounted in epoxy. (b) The mount was grinded and polished until a large portion of each apatite grain has been exposed. (c) Chemical etching (dilution HNO3) has been done to reveal the spontaneous fission-tracks (description in text). The confined tracks below the surface can be revealed only if there is a pathway for the etchant (a surface track, cleavage, or fracture) to penetrate. (d) External detector mica has been mounted in close contact with the polished grain mount. (e) This sandwich has been sent to a nuclear reactor. Here, the sample has been irradiated with low-energy thermal neutrons, which induced fission in ^{235}U. During the fission process, heavy particles crossed the interface between the mineral and the mica, producing a mirror image of the original grain. (f) After irradiation, the mica has been removed and chemically etched to reveal the induced tracks. (g) Grain mounts and micas have been mounted on a glass slide as mirror image and track densities can be estimated under microscope (modified after Gallagher et al., 1998; Hendriks, 2003).

tracks take place progressively and is influenced by factors such as temperature, time (Wagner, 1968; Fleischer et al., 1975), chemical composition and crystal anisotropy (Barbarand et al., 2003). Fleischer et al. (1965 and 1975) shown that temperature is the only relevant factor in controlling annealing, and since, it has been used as thermal annealing.

At geological timescales, fission-tracks formed in apatite anneal completely at temperature >110°±10°C for a resistance time of 10^6-10^7 years (Gleadow and Duddy, 1981; Green et al., 1986). This temperature is defined as "closure temperature", below which fission-tracks anneal progressively until 60°±10°C. This temperature interval is referred to as the Partial Annealing Zone (PAZ; Fig. 3.8; Gleadow and Duddy, 1981; Naeser, 1981). From ~60° to surface temperature, the annealing is supposed to be negligible (Carlson, 1993; Laslett et al., 1987; Wagner, 1968). However, spontaneous tracks, measured in the natural samples that rapidly cooled through the PAZ and remained close to the surface temperature since their formation (e.g. volcanic ash), have a mean track length of 14-15 µm. It is shorter with 1-1.5 µm than the induced tracks (Gallagher et al., 1998) and is due to the result of the natural annealing over millions of years (Vrolijk et al., 1992).

Thermal annealing can be controlled by additional factors such as the track orientation with respect to the crystallographic c-axis and chemical composition. Track lengths shorten at a different rate depending on the orientation of the track relative to the crystal c-axis. Fission-tracks parallel to the crystallographic c-axis shorten faster then those found at a higher angle because the etchant penetrates faster along the c-axis (Crowley et al., 1991; Donelick, 1991). Chemical composition of an apatite crystal might vary the upper thermal benchmark of the PAZ up to 200°C (Ketcham et al., 1999; Murrell, 2003). Tracks in a pure fluor-apatite anneal more quickly then those in a chlorine apatite (Galbraith and Laslett, 1993). In order to distinguish if the samples have Cl-rich or Fl-rich apatite, it is necessary to measure the diameter of the etch-pits from those grains which have been counted (Carlson, 1993; Donelick, 1991).

3.4.3. Sample preparation and analytical dating procedure

After the mineral separation (Fig. 3.11) and selection of apatites for (U-Th)/He dating were done, the remaining grains have been used for fission-track analysis. Various analytical dating techniques developed over the time have been applied for age determination (Gleadow, 1981). In this study, the External Detector Method has been used (EDM; Gleadow and Duddy, 1981). This method has the advantage that the exact same area is used to determine the density of spontaneous and induced tracks (necessary for age determination) and that the variation of individual grains ages can be evaluated.

Two grain samples were prepared: one to determine the fission-track density (ca. 20-50 grains) and one to measure the track length distribution (~100-150 grains). The grains mounted in epoxy have been sent to the reactor for irradiation (Fig. 3.15).

(a). The mount was grinded and polished until a sufficiently large portion of each apatite grain was exposed *(b)*. Before sending the mount to the reactor, the spontaneous tracks in apatites were revealed by chemical etching in 1.5 N HNO_3 at a temperature of 21°C for 35 seconds *(c)*. Tracks below the surface are revealed if there is a pathway for the etchant (a surface track, cleavage, or fracture) to penetrate. A low-U muscovite external detector (EDM) was mounted in close contact with the polished grain mount *(d)*. This sandwich was sent to the low flux nuclear reactor of ECN (Petten, NL). Here, the sample was irradiated with low-energy thermal neutrons for 14 hours, which induced the fission of ^{235}U *(e)*. During the fission process, part of the heavy particles from the induced fissions in the mineral reached the mica, producing mirror images of the original grains *(e)*. The neutron flux was monitored by two dosimeter glasses with a known U-content placed at the top and the bottom of the two sets of samples. For this study, the CN5 glass was used (12 ppm U). Subsequently to irradiation, the micas were removed from the apatite grain

mounts and dosimeter glasses, and were chemically etched to reveal the induced tracks *(f)*. Mica from each sample was etched in 48% HF for 12 minutes in order to reveal the induced tracks produced by the fission of ^{235}U in the glass dosimeter. Grain mount and corresponding mica were mounted on glass slides as mirror image *(g)*. Determination of spontaneous and induced track densities (ρs and ρi) was carried out using a microscope with a stage.

3.4.4. Age calculation

The fission-track method is based on the constant fission of ^{238}U. In order to calculate the time *t*, the fission-track age, the number of spontaneous tracks has to be determined per unit of volume. The number of ^{238}U is derived from the number of induced tracks counted on the mica external detector. Age equation for fission-track dating requires basically an estimation of the relative abundance of the parent and daughter product. This is represented by the total amount of uranium that is present within the apatite grain (^{238}U atoms) and the number of the spontaneous fission-tracks that have accumulated in time within a mineral, per unit volume. The latter is directly counted on a polished and etched internal surface in an apatite crystal. The former is derived from counting the induced tracks, which are formed by irradiating a sample with low energy-thermal neutron flux that induces fission in ^{235}U. Due to the fact that ratio $^{235}U/^{238}U$ is constant in nature, the ^{238}U parent distribution can be easily determined.

Apatite fission-track age equation is written as (Price and Walker, 1963; Naeser, 1967):

$$Age = \frac{1}{\lambda_D}\ln\left[1 + \frac{\rho s \lambda_D \sigma I \phi g}{\rho i \lambda_F}\right] \qquad (3.4.1.)$$

where λ_D is total decay constant for ^{238}U (1.551×10^{-10} yr^{-1}); λ_F is decay constant for spontaneous fission of ^{238}U (values are clustered around 7×10^{-17} yr^{-1} and 8.5×10^{-18} yr^{-1}; Wagner and van den Haute, 1992); σ is cross-section for thermal neutron-induced fission of ^{235}U (584.25×10^{-24} cm^2); I is isotopic ratio $^{235}U/^{238}U$ (7.252×10^{-3}); Φ is thermal neutron fluence (neutron/cm^2); ρ_i is neutron-induced track density from ^{235}U (track/cm^2); ρ_s is spontaneous track density from ^{238}U (track/cm^2); g is geometry factor (0.5 for EDM; Wagner and van den Haute, 1992). Values of constants λ_D, σ, I and g are well established, track densities ρ_i and ρ_s are directly derived from counting the fission-tracks on the apatite grain and mica mounts.

3.4.4.1. Zeta age calibration

Hurford and Green (1982, 1983) showed that the absolute values of the decay constant λ_F and of the thermal neutron fluence Φ are problematic to be determined separately because each value depends on each other. The zeta method ζ has been adopted to overcome this problem. In principle, the fission-track age of a sample with unknown age is calibrated against one or more known age standards. First, the age standards are irradiated and analysed together with uranium bearing glass monitor (dosimeter) in order to determine a calibration factor ζ. This factor is given by a combination of λ_F and Φ. Induced track density ρ_d for each standard is a measure of thermal neutron fluence. The ratio between thermal neutron fluence Φ and induced tracks ρ_d is:

$$\phi = B\rho_d \qquad (3.4.2.)$$

where constant B represents the proportionality between neutron fluence and in-

duced tracks. If the constant is introduced in the age equation (3.4.1.), then this can be rewritten as:

$$Age = \frac{1}{\lambda_D}\ln\left[1 + \frac{\rho s \lambda_D \sigma B \rho_d \phi g}{\rho i \lambda_F}\right] \quad (3.4.3.)$$

where ρ_d is fission-track density in the external detector mica, which covers the glass dosimeters during irradiation (tracks/cm²). ζ for a particular dosimeter glass is defined as:

$$\zeta = \frac{\phi \sigma I}{\lambda_F \sigma_d} \quad (3.4.4.)$$

At lengths, the equation (3.4.1.) becomes:

$$\zeta = \frac{(e^{\lambda_D T_{std}} - 1)}{\lambda_D \left(\frac{\rho s}{\rho i}\right)_{std} g \rho_d} \quad (3.4.5.)$$

where T_{std} is standard age and (ρ_s/ρ_i)std is the fission-track density ratio resulted from spontaneous and induced tracks of a standard mineral. From the above equation, a personal ζ value is obtained for each standard age and glass (dosimeter). This value becomes normally constant in time after repeated measurements and indicates that the analyst is consistent in time in determination of the track density, which guarantees the reproducibility of the analyses. After a personal ζ value is obtained, the unknown age for each apatite grain can be computed using the following equation:

$$Age = \frac{1}{\lambda_D}\ln\left[1 + cf\frac{Ns}{Ni}\right] \quad (3.4.6.)$$

where $cf = g\lambda_D \zeta \rho_d$ is the correction factor. (3.4.7.)

In this study, the zeta was determined using two Fish Canyon Tuff standards (Colorado, U.S.A.), which have an age of 27.9±0.5 Ma (Schmitz and Bowring, 2001). The obtained personal weighted mean ζ-value is 337.5±28.4 (Table 3.4). The error associated to the ζ-factor was calculated as follows (Green, 1981):

$$\sigma(\zeta) = \zeta\sqrt{\frac{1}{N_s} + \frac{1}{N_i} + \frac{1}{N_d} + \left[\frac{\sigma(T_{std})}{T_{std}}\right]^2} \quad (3.4.8.)$$

where N_s, N_i and N_d are numbers of spontaneous, induced and glass dosimeter tracks counted and σ is the standard error.

3.4.4.2. Pooled, mean and central ages

Typically, between 20-40 apatite grains have been counted for each sample in order to calculate the fission-track age. This age can be expressed as pooled, mean and central age. The *mean age* results from the arithmetic average of the single-grain ages, while the *pooled age* is based on the Poissonian statistics (*P*). It presumes that all apatite grains from one sample have a common true age (belong to a single population). This assumption can be easily tested by doing the $P(\chi^2)$ test (Galbraith, 1981), which is the Chi-squared probability of single-grain ages in %. If $P(\chi^2)$ has a value >5%, it points out that all grains experienced similar thermal history (equally annealed) and belong generally to a homogenous age population (pooled age; Galbraith and Laslett, 1993), which can be interpreted in the terms of exhumation (Gleadow et al., 1986). If $P(\chi^2)$ is <5%, it indicates that that

sample has a wide-spread age distribution, having mixed ages (multiple populations).

The *central age* (Galbraith and Laslett, 1993) is defined as mean of the logarithmic distribution of single grain ages, weighted by the precision of the individual measurement. Galbraith and Laslett (1993) introduced the *age dispersion* term for a better interpretation of the ages. It indicates the relative standard deviation σ of population age (in %). Dispersion <0.10 (10%) indicates that the grain age distribution probably corresponds to an age group, while a value >0.40 (40%) points to a considerable heterogeneity, e.g. multiple age populations.

3.4.4.3. Graphical assessment and decomposition of spread in an AFT age (radial plots)

Fission-track single age data are plotted as radial plots (Galbraith, 1990). The *Y* axis represents the age standardised estimate ($y_j=(z_j-z_0)/\sigma_j$), while the *X* axis represents the precision ($1/\sigma_n$). The precision is proportional to the number of the induced and spontaneous tracks per single grain. Fission-track age is shown millions of years (Ma) on the *Z* axis, usually represented as a semicircle to show the central age, which is placed at the centre of the arc. The semicircular *Z* scale has a log age scale. However, for those samples with low spontaneous or induced tracks, the arcsin age scale is more advisable (Galbraith, 1990).

In the radial plot, the individual grain ages are plotted together with their standardised estimated (y_j), standard error ($z_j\pm2\sigma$) and precision ($1/\sigma_n$) values. For any grain (X,Y), the corresponding age (Z_n) can be read on the semicircular scale by extrapolating a line from ($0,0$) through (X,Y) (Fig. 3.16a). The individual two-sigma confidence interval on the single grain age can also be drawn by extrapolating two lines from the origin ($0,0$) through the $\pm2\sigma$ single age error bar, (($X_j,Y_j,Z_j+2\sigma$) and ($X_j,Y_j,Z_j-2\sigma$)). To avoid displaying all the grain error bars, the associated standard error ($\pm2\sigma$) for the central age is shown by the truncated ends of the *Y* axis, which allows the visual evaluation of all grain estimate distributions (Fig. 3.16a).

For those samples with spread in age distributions (did not pass the $P(\chi^2)$ test), the BinomFit software can be used to identify different age components (populations; Brandon, 1992). It can result in one or more components, which can be visualised as groups of single-grain ages gathered around regression lines in a radial plot (Fig. 3.16b). The youngest component is called *minimum age* and was introduced by Galbraith and Laslett (1993). For non-reset samples, it can be used as a proxy for the depositional age (Brandon and Vance, 1992; Garver et al., 1999), while for reset ones, it corresponds to that part of grains which annealed faster due to the chemical composition (Green et al., 1986; Green et al., 1989). Results obtained for samples analysed during this study are reported and explained in Subchapter 5.3.

3.4.4.4. Measurements of fission-track lengths and etch-pits (D-par)

Fission-track length is an important parameter because the length decreases with increasing temperature and can be used to estimate the degree of annealing (Wagner and Storzer, 1972). The best representation of true fission-track lengths is given by measuring those tracks that are completely contained within the host mineral (confined tracks; Gleadow et al., 1986) and are etched from the intersection with another track (TINT; Bhandari et al., 1971) or fractures (TINCLE; McDougall et al., 1971). In this study, both

Figure 3.16

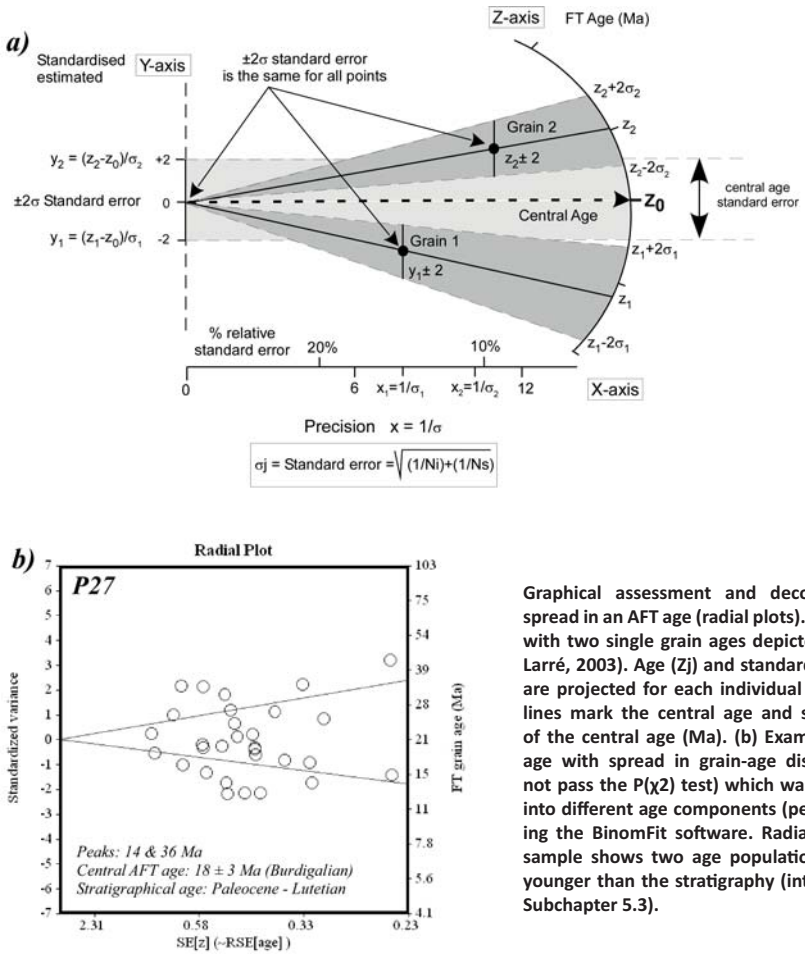

Graphical assessment and decomposition of spread in an AFT age (radial plots). (a) Radial plot with two single grain ages depicted (after Juez-Larré, 2003). Age (Zj) and standard error (Zj±2σ) are projected for each individual grain. Dashed lines mark the central age and standard error of the central age (Ma). (b) Example of an AFT age with spread in grain-age distribution (did not pass the P(χ2) test) which was decomposed into different age components (peaks) by applying the BinomFit software. Radial plot for this sample shows two age populations, older and younger than the stratigraphy (interpretation in Subchapter 5.3).

TINT and TINCLE track lengths have been measured on surfaces parallel to the c-axis of the apatite crystal. Orientation of tracks, the angle they make with c-axis, has also been considered because those tracks which are parallel to the c-axis anneal faster (longer tracks) than those which are perpendicular or at a different angle (shorter tracks). Only the confined tracks situated at angles <100 with respect to the polished surface have been considered.

The limited number of measurable confined tracks observed during counting of the Carpathian samples (5-10 per sample), similar to the earlier study of Sanders (1997), would have prevented to constrain adequately the thermal histories. Consequently, a second mount was prepared for each sample, further being irradiated with fragments from a Californium source allowing deeper etching. The Californium irradiation was performed by R. Donelick, Donelick Analytical, Inc., using a ^{252}Cf source (U.S. Geological Survey). Here, the mounts were irradiated with Californium (Cf) for many hours in order to create small holes into the apatite grains necessary for the etchant to penetrate. During the irradiation, the samples were placed under an Isotope Products Laboratories µmCi ^{252}Cf source (FF-252-4) at a distance of 8.2 cm below the active surface. Then, the irradiation apparatus including the ^{252}Cf source and the specimens were placed under a near

vacuum (<666 Pa) for a total period of 68 h 5 min (Wendt et al., 2002). Subsequently, the confined tracks were revealed by etching the apatites with 1.5N7% HNO_3 for 35 seconds at a constant temperature of 21°C. The number of confined tracks per sample increased with one order of magnitude using this procedure, e.g. from 5-10 to ~80-100 tracks.

Grains of a sample might experience differential annealing due to variable chemical compositions (Green et al., 1986; Green et al., 1989). Chemical composition of an apatite can be revealed by measuring the size of the etch-pits (D-par method). Therefore, apatites with etch-pits bigger than 1.75-2.0 µm (Cl-rich) are more retentive for fission-tracks, while those with etch-pits smaller than 1.75 µm (Fl-rich) are more sensitive to annealing (Carlson, 1993; Donelick, 1991). In this study, the etch-pits have been measured on the same grains counted for spontaneous tracks (Table 5.1). The mean values of the measured etch-pits indicate that Cl-rich apatites are present in the Baraolt and Marginal Folds nappes, Fl-rich apatites in the Ceahlău and Subcarpathian nappes and more Cl- and less Fl-rich apatites in the Bucovinian and Tarcău nappes and on the western flank of the Focşani basin.

A relationship cannot be directly traced between the fission-track length and the size of the etch-pits mainly because part of the samples are not reset for AFT (e.g. Subcarpathian nappe and western flank of Focşani basin) or ages are close to the stratigraphy (e.g. Bucovinian nappe), conditions when the older fission-tracks are preserved and prevent to make a realistic interpretation. In samples from the Marginal Folds, Baraolt and Ceahlău nappes, track lengths are comparable for different etch-pit values (Table 5.1). Only in samples from the Tarcău nappe, it can be observed that fission-tracks are slightly longer in Cl-rich samples than in the Fl-rich ones. Because no track lengths were measured in the Fish Canyon Tuff standards, additional information cannot be provided.

Computer controlled-microscope stage Autoscan Systems was used to perform the age determination, length and etch-pit measurements (Autoscan Systems Ply. Ltd. 2002). A 100x10 magnification has been used during the counting and the length measurements. At length, the data being exported to Trackkey for further analysis.

3.5. Thermal modelling for apatite fission-track and (U-Th)/He methods

Thermal history experienced by a rock sample is reconstructed by means of thermal modelling, which generally integrates the AFT age and the track length distribution. Several models have been proposed aiming to model the kinetics of the track annealing in different apatites, based on the results obtained from laboratory annealing experiments: Durango Flour-Chlorapatite (Carlson, 1990; Laslett et al., 1987; Crowley et al., 1991), Flourapatite and Flour-Strontium apatite (Carlson, 1990; Crowley et al., 1991) and composite models (Ketcham et al., 1999). All these models incorporate the relationship between fission-track shortening and density reduction given for t-T conditions.

The annealing model of Laslett et al. (1987) is commonly used in thermal history studies because fits best to the natural data. However, careful attention has to be paid during modelling because "a Late Neogene cooling effect" can be introduced. This effect occurs because of the initial track length parameter (l_o) in the annealing model is based on the mean length of the induced tracks, which has a l_o with 1-1.5 µm longer than the spontaneous tracks measured in samples, which remained at the surface since their formation. This problem might be overcame by reducing the initial track length parameter in the

thermal model prior to any attempt to model, which was not consider during this study.

Two modelling procedures can be used to reconstruct (model) the thermal history of a rock sample using an AFT age and track length distribution (including the He age in this study): forward and inverse modelling. The former generates a particular FT age and a track length distribution from a t-T path defined by the modeller. The results are then compared with the AFT data collected from a rock sample to check if the output fits with the AFT data. The inverse modelling is based on generation of multiple forward models, which assume to fit to a particular AFT age of a rock sample, for this study the approach is based on the probability, genetic algorithms (Monte Carlo approach; Gallagher et al., 1991). The degree of fitting with the AFT age and length distribution are evaluated with the P(χ2) test and the Kolmogorov-Smirnov (K-S) statistical indicators, respectively (Ketcham et al., 1999).

Thermal modelling of samples analysed during this study has been carried out using the HeFTy software (Ketcham et al., 1999), using the Laslett et al. (1987) annealing model. Inverse modelling was performed to generate the best statistical t-T paths for each sample by incorporating parameters such as: stratigraphy, AFT and (U-Th)/He ages, track lengths, etch-pits (D-par), surface temperature and two geological constrains, namely Oligocene exhumation and Pliocene subsidence. The geological basis of these parameters (boxes) and the role they play in steering the t-T paths are further explained in Subchapter 5.3.2. The modelling results are given as grey coloured areas (or envelops), each describing the degree of best fit. The external envelop (dark grey) stands for acceptable paths, the internal one (light grey) stands for good paths, while the best fitting path is shown as a dashed black line (Fig. 3.17).

The degree of annealing for each track was calculated based on the ratio between the initial track length (*Lo*), the measured track length (*L*) and its angle with the c-axis. The initial track length was around 16.3 µm. 100.000-150.000 random time-Temperature paths were generated per modelling run. The predicted (modelled) AFT ages and length distributions have been compared with the measured ones and only those having the

Figure 3.17

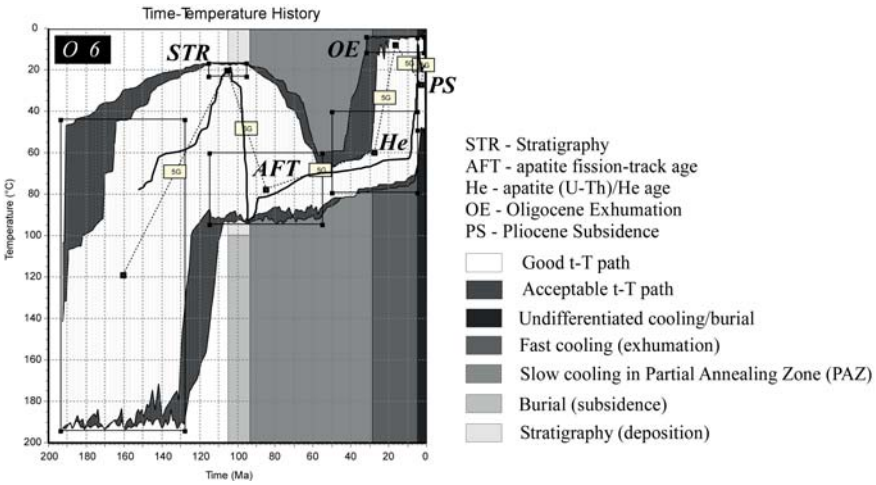

Thermal modelling done for sample P4 with HeFTY software.

goodness of fitting (GOF) higher or close to a value of 0.70 were considered reliable for the geological interpretation.

Prior to HeFTy modelling, DECOMP software was applied to compute the He age evolution curves of apatite grains with various geometries for several samples (Meesters and Dunai, 2002). This method is used for solving the production-diffusion equations for finite diffusion domains of various shapes and arbitrary cooling histories. The surface to volume ratio of mineral grains of different shapes and aspect ratios is an important parameter describing the influence of geometry on diffusion behavior. Two to five grains with either spherical or hexagonal geometries (Fig. 3.12a-d) have been analysed per sample (Fig. 3.13a-b), the hexagonal geometries being converted to a spherical one based on the surface to volume ratio (Table 3.2). The analysed grains were: fully reset for helium in samples P4, P8, P25, P26, P27, P28, O3, O6, O7, O8 and O13; partially reset in sample P7, P9, P10, P11 and O1; and not reset in samples P6, P12, P13, P14 and P18. The He age evolution curves could not be accurately modelled even for the fully reset grains probably due to large spread of obtained individual ages within the distribution of each reset sample. Therefore, these results not further discussed were neglected from the interpretation.